Article

Effect of Er, Si, Hf, Nb additives on the thermal stability of microstructure, electrical resistivity and microhardness of fine-grained aluminum alloys Al-0.25%Zr

A.V. Nokhrin [1,*], G.S. Nagicheva [1], V.N. Chuvil'deev [1], V.I. Kopylov [1], A.A. Bobrov [1], N.Yu. Tabachkova [2,3]

[1] Materials Science Department, Physical and Technical Research Institute, Lobachevsky State University of Nizhny Novgorod, 603022, Nizhny Novgorod, Russia; nokhrin@nifti.unn.ru (A.N.); nagicheva@nifti.unn.ru (G.N.); chuvildeev@nifti.unn.ru (V.C.); kopylov@nifti.unn.ru (V.K.); bobrov@nifti.unn.ru (A.B.).

[2] Center Collective Use "Materials Science and Metallurgy", National University of Science and Technology "MISIS", 119991, Moscow, Russia; ntabachkova@misis.ru (N.T.)

[3] Laboratory "FIANIT", Laser Materials and Technology Research Center, A.M. Prokhorov General Physics Institute of the Russian Academy of Sciences, 119991, Moscow, Russia; ntabachkova@gmail.com (N.T.)

* Correspondence: nokhrin@nifti.unn.ru (A.N.)

Abstract: The conductor aluminum alloys Al-0.25wt.%Zr doped additionally with X = Er, Si, Hf, and Nb were the objects of investigations. The fine-grained microstructure in the alloys was formed by Equal Channel Angular Pressing and Rotary Swaging. The thermal stability of the microstructure, specific electrical resistivity, and microhardness of the novel conductor aluminum alloys was investigated. The mechanisms of nucleation of the $Al_3(Zr,X)$ secondary particles during annealing the fine-grained aluminum alloys were determined using Jones-Mehl-Avrami-Kolmogorov equation. Using Zener equation, the dependencies of the mean secondary particle sizes on the annealing time were obtained on the base of analysis of the data on the grain growth in the aluminum alloys. The secondary particle nucleation during long-time low-temperature annealing (300 °C, 1000 hrs) was shown to go preferentially at the cores of the lattice dislocations. The Al-0.25%Zr-0.25%Er-0.20%Hf-0.15%Si alloy subjected to long-time annealing at 300 °C has the optimal combination of the microhardness and electrical conductivity (59.8%IACS, Hv = 480 ± 15 MPa).

Keywords: Aluminum alloys; Al-Zr; microstructure; electrical conductivity; microhardness; diffusion.

1. Introduction

At present, high-strength aluminum alloys with increased electrical conductivity are considered as substitutes for copper alloys applied widely for making the fine wires (∅0.2-0.5 mm) of the on-board wiring of modern aircrafts and automotive. International companies use fine bimetallic wires copper-clad aluminum wires made from complex aluminum alloys for novel airplane and automotive electrical wiring [1-5]. The fine aluminum wires can be applied efficiently also in car-building industry, electric power engineering, power transmission applications, etc. High strength and electrical conductivity are the key characteristics of the conductor aluminum alloys. At usual methods of processing of commercial purity aluminum or ultra-low-doping commercial aluminum alloys, high strength and electrical conductivity are hardly compatible [6-16]. One of approaches to the development of novel conductor aluminum alloys is their doping with the elements, which affect the electrical conductivity weakly but affect their strength positively. In Russia, highly doped eutectic alloy 01417 has been developed, the fine copper-clad aluminum wires from which are applied extensively in cable industry at present [17-20]. For example, industrial alloys 01417 have the minimal ultimate strength 160 MPa, relative elongation 8%, and specific electrical resistivity (SER) 3.2 μΩ·cm [17]. At present, novel highly doped eutectic aluminum alloys doped with Ce and La is being developed extensively [21-27].

Preprints (www.preprints.org) | NOT PEER-REVIEWED | Posted: 22 December 2022 doi:10.20944/preprints202212.0407.v1

Modern automotive and aviation technology imposes more and more high requirements to the fine wires in strength and thermal stability of the microstructure, which cannot be met using commercial aluminum alloys anymore. In this connection, aluminum alloys modifications of Al-Mg-Si system alloys [11, 16, 28-36] (commercial alloys of 6XXX series [28, 32, 33, 36, 38-40], Al-Mg-Si-Zr alloys [30], Al-Mg-Si-(Ni,Fe) + (Sc,Zr) [37], Al-Mg-Si-Cu [41], et al.), conductor alloys Al-Fe [8, 42-44] and novel aluminum alloys multi-doped with various rare earth elements (REEs) and transition metals (TMs) – zirconium, scandium, hafnium, yttrium, etc. are being developed extensively [45-56].

Earlier, the investigations have demonstrated the Sc-containing aluminum alloys have high strength and thermal stability characteristics [45, 48, 49, 51, 52, 54, 57-67] but wide application of these ones is limited by high cost of Al-Sc ligature. This makes the problem of development of aluminum alloys economically doped with scandium as well as development of alloys, which expensive scandium is replaced by microadditives of cheaper REE and TM relevant [61-63].

At present, investigations on development of the conductor alloys in Al-Zr system are being carried out extensively [68-74]. The increased temperatures and times of nucleation of Al_3Zr particles (about 50-100 hrs at the temperatures over 350 ^oC) is a disadvantage of this system from the viewpoint of prospects of application as the heat-resistance wires. This doesn't allow providing the stabilization of nonequilibrium fine-grained microstructure in the wires during long-term operation at ~180-220 ^oC whereas preliminary annealing for the nucleation of the secondary particles reduces the technological plasticity of the workpieces often and limits the opportunity to make the fine wires by rolling at reduced temperatures. To solve this problem, Al-Zr alloys are applied with zirconium concentration up to 0.4-0.6 wt.%, which are made using special ultrafast crystallization technologies [68, 69, 71-75]. Second, more efficient way is additional microdoping of Al-Zr alloys by the elements (most often – Er [45, 49, 50, 56, 76-83], Hf [49, 56, 75, 77], Y [49, 50, 84-87], Yb [50, 88-90], et al.) providing accelerated decomposition of solid solution at lower annealing temperatures. Note that additional doping allows avoiding the intermittent decomposition of solid solution, which are observed in Al-Zr alloys often [91-95].

In the present work, we investigated the effect of Er, Hf, Nb, and Si additives on the thermal stability of microstructure in Al-Zr alloys. The choice of Er and Hf was caused by positive effect of these ones on the acceleration of nucleation of Al_3Zr secondary particles in Al-Zr alloys [56, 75, 78-83]. Doping of aluminum with niobium allows forming the Al-Nb particles with $D0_{23}$ structure and also allows controlling the character of distribution of Al_3Zr particles and forming the AlZrNb secondary particles additionally [96]. The choice of Si as a doping element was caused by its effect on the kinetics of nucleation of secondary particles. Si is capable to accelerate the nucleation of the secondary particles in aluminum alloys containing the combinations of metals Al–Hf and Al–Zr [90]. The highest concentration of zirconium in the alloys investigated is limited to 0.25%Zr since large primary Al_3Zr particles are formed in the alloy at higher concentrations. These particles can be the sources of акфсегку of the fine wires of 0.2-0.5 mm in diameter during fabrication by various cold deformation methods (drawing, rolling, etc.). Note also that the formation of the Al_3Zr particles at higher zirconium concentrations goes via discontinuous precipitation of solid solution mechanism often [91-95]. As a consequence, their contributions into the strength and thermal stability of the aluminum wires decrease.

The present work was aimed at the investigation of the effect of the micro additives of Er, Si, Hf, and Nb on the thermal stability of the conductor aluminum alloys Al-0.25%Zr, the fine-grained microstructure in which was formed combining the technologies of Equal Channel Angular Pressing (ECAP) and Rotary Swaging. The application of ECAP and Rotary Swaging technologies allows eliminating the dendrite nonuniformity of the cast macrostructure of the aluminum alloys as well as forming a uniform fine-grained microstructure in the aluminum alloy. It allows forming the microstructure in the aluminum alloys, the parameters of which are similar to the microstructure of fine bimetallic wires made by rolling, extrusion or drawing [1-5, 25, 57, 58]. It should be stressed here that the formation of the fine-grained microstructure affects the intensity and

Preprints (www.preprints.org) | NOT PEER-REVIEWED | Posted: 22 December 2022 doi:10.20944/preprints202212.0407.v1

mechanisms of nucleation of the secondary particles (Al_3Sc, Al_3Zr, etc.) in the aluminum alloys [59, 60] and also affects many mechanical properties and performance characteristics of the aluminum alloys (strength and hardness, fatigue resistance, ductility at room and elevated temperatures, etc.) positively [7, 12, 14-16, 23, 26, 29, 32, 33, 36-39].

The applied goal of the work was achieving the SER of 3.0 μΩ·cm or less in the novel conductor alloys with simultaneous ensuring a high microhardness of these ones.

2. Materials and Methods

The aluminum alloys, the compositions of which are presented in Table 1 were the objects of investigations.

Table 1. Compositions of the aluminum alloys.

Alloy #	Contents of doping elements in the alloys, wt.%				
	Zr	Er	Si	Hf	Nb
1	0.25	0.25	0.15	0.2	-
2	0.25	0.25	0.15	-	-
3	0.25	-	0.15	-	-
4	0.25	-	-	0.15	-
5	0.25	-	-	0.25	-
6	0.25	-	-	-	0.15

The workpieces of the aluminum alloys of 20×20×160 mm in sizes were obtained by induction casting with Indutherm® VTC-200V casting machine in vacuum in the regimes specified in Table 2. To prepare the alloys, aluminum A99 as well as Al-3%Zr, Al-3%Hf, Al-3%Si, Al-3%Er, and Al-2%Nb master alloys, obtained by the induction casting followed rolling into foils of 0.2 mm in thickness were used.

Table 2. Casting regimes for the aluminum alloys.

Casting regimes	Alloy #					
	1	**2**	**3**	**4**	**5**	**6**
Copper mistress, mm	22×22×160					
Ceramic crucible volume, cm^3	150					
Purging by argon prior to melting, cycles	3					
Purging by argon during heating, cycles	3					
Melt mixing	Induction					
Cooling down, s	250 –50 under vibration					
Heating power, kW	4.5					
Time to the melting of the components	8 min 25 s	7 min 35 s	7 min 55 s	8 min 5 s	8 min 20 s	8 min 12 s
Melt temperature, °C	800					
Holding time prior to casting, min	20					
Casting temperature, °C	780					

The workpieces obtained were subjected to N = 4 ECAP cycles at 250 ºC. ECAP was performed according to "A" scheme using hydraulic press Ficep® HF400L (Italy) in square cross-section hardware with the channel crossing angle 90º. The strain rate in ECAP was 0.1 mm/s. After ECAP, the samples were subjected to Rotary Swaging at room temperature using a machine manufactured by R5-4-21 HIP "Heinrich Muller Maschinfabrik" Company (Germany). The rod samples with initial diameters of 20 mm were subjected to Rotary Swaging down to the diameters of 6.0 mm. The overall strain of the rods was 70%. The obtained cylindrical samples of 6 mm in diameter and 12 mm long were subjected to

Preprints (www.preprints.org) | NOT PEER-REVIEWED | Posted: 22 December 2022 doi:10.20944/preprints202212.0407.v1

sediment up to the strain of 35%. The sediment was performed at room temperature (RT) using a 40-ts hydraulic press EU-40 (Germany).

As a result of application of sediment, the samples of 10 mm in diameter were made suitable for measuring the specific electrical resistivity (SER) by eddy current method using SIGMATEST 2.069 device with the sensor of 8 mm in diameter. The uncertainty of measuring the SER was ±0.03 μΩ·cm. The measurements of microhardness (Hv) were performed using HVS-1000 hardness tester at the load of 50 g. The mean uncertainty of measuring Hv was ± 15 MPa.

To carry out the investigations of macro- and microstructure of the alloys Leica® DM IRM metallographic microscope, Jeol® JSM-6490 scanning electron microscope (SEM) with Oxford Instruments® INCA 350 EDS microanalyzer, and Jeol® JEM-2100F transmission electron microscope (TEM) were employed. The samples were subjected to mechanical grinding and polishing in advance using diamond pastas of different dispersion as well as to electrochemical polishing at the finishing stage (current 3 A, voltage 30 V, 1 min) in CrO_3+H_3PO_4 electrolyte. The microstructure of the alloys was revealed by etching in HF (15 ml) + HNO_3 (10 ml) + glycerin (35 ml) solution. The volume fraction of the recrystallized microstructure f_R and the mean grain sizes d were determined by grain intersection counting method using GoodGrains software (Russia, UNN). The mean uncertainty of determining the magnitude of f_R was ±1 vol.% and the mean relative uncertainty of determining the mean grain sizes was ~10% of its magnitude d.

To investigate the thermal stability of the microstructure, the samples were subjected to annealing in air ambient using EKPS-10 furnace (Russia). The annealing was performed in two regimes: (a) 60-min annealing in the range from the RT up to 550 °C; (b) isothermal annealing at 300°C for up to 1000 hrs. The precision of maintaining the temperature (T) in the furnace was 10 °C. The samples were placed into the furnace on the ceramic furnace heated up to required temperature in advance. Cooling the samples after annealing was performed in air.

3. Results

3.1. Investigation of the alloys in the initial state

Fig. 1 presents the images of microstructure of the aluminum alloys investigated. The specimens for investigations were taken from the lower parts of the bulks.

(**a**) (**b**) (**c**)

Preprints (www.preprints.org) | NOT PEER-REVIEWED | Posted: 22 December 2022 doi:10.20944/preprints202212.0407.v1

(d) (e) (f)

Figure 1. Macrostructure of the cast aluminum Alloys #1 (a), 2 (b), 3 (c), 4 (d), 5 (e) and 6 (f). The numbers in the figures correspond to the numbers of alloys in Table 1. Optical microscopy.

The macrostructure of the cast alloys comprises a mixture of columnar crystals at the edges of the samples and the equiaxial grains in the central parts of the bulks. The ratio of the areas occupied by the equiaxial grain zones and by the columnar crystal ones depends on the concentrations of the doping elements. The largest area in the cross-section occupied by the equiaxial grains of 10-50 μm in sizes was observed for Alloy #1 containing the highest concentration of the doping elements.

Figures 2 and 3 present the results of SEM investigations of the composition and the character of distribution of the primary particles in the macrostructure of the cast (Fig. 2) and deformed aluminum alloys (Fig. 3).

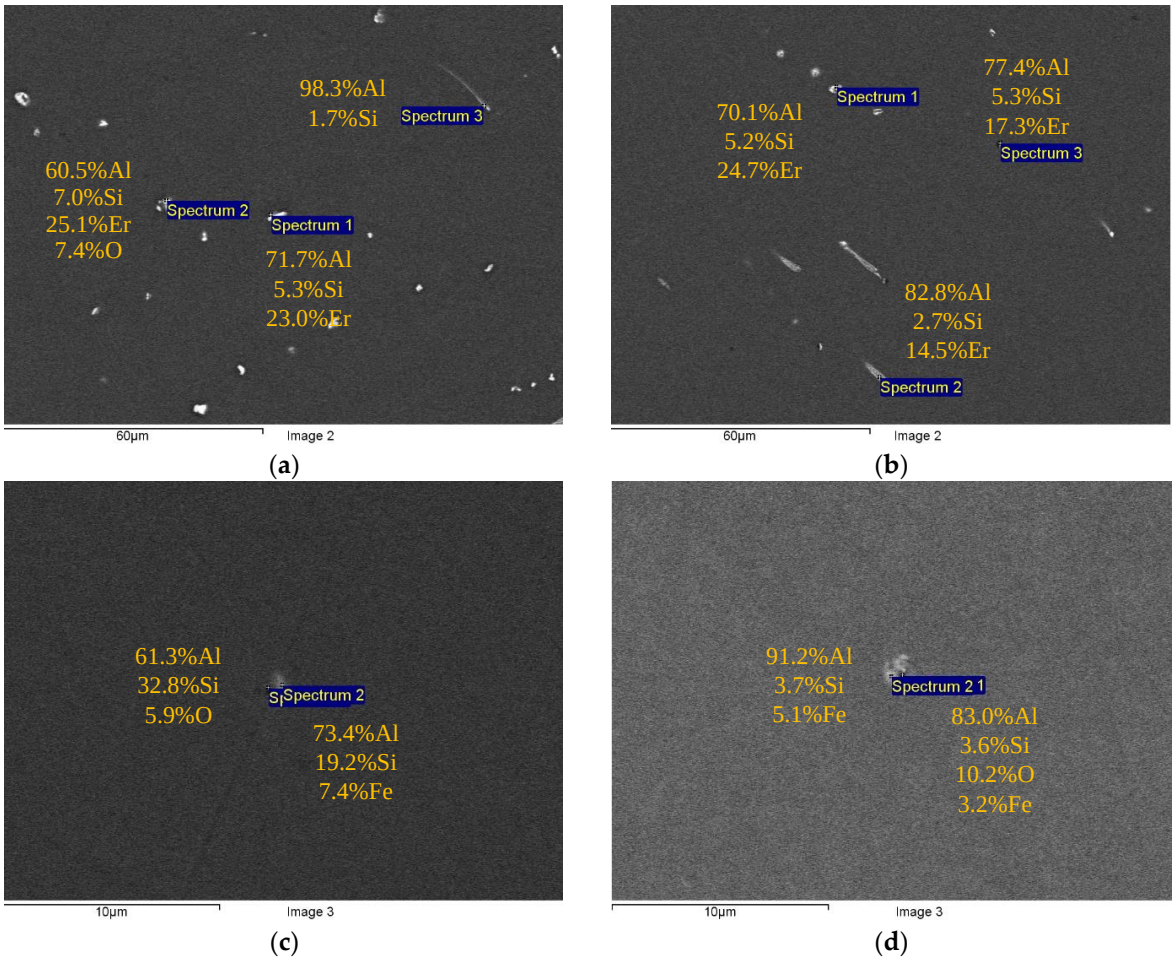

Preprints (www.preprints.org) | NOT PEER-REVIEWED | Posted: 22 December 2022 doi:10.20944/preprints202212.0407.v1

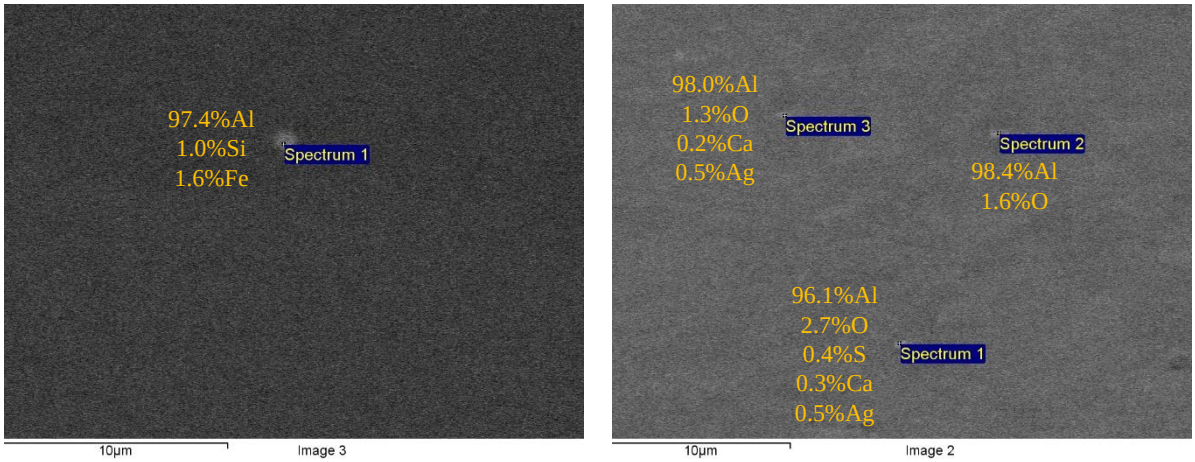

(**e**) (**f**)

Figure 2. EDS microanalysis of the composition of the primary particles in the cast Alloys #1 (**a**), #2 (**b**), #3 (**c**), #4 (**d**), #5 (**e**), and #6 (**f**). SEM.

One can see the chains of light particles in the macrostructure of the cast Alloys #1 and #2. The large elongated particles are located preferentially at the dendrite boundaries exhibiting another contrast in the SEM investigations. Inside the dendrites in Alloy #2, there are many micrometer-sized particles, the shapes of which are close to the equiaxial ones. The results of the EDS microanalysis show Al, Si, and Er to present in the composition of the particles in different proportions (Fig. 2a, b). In Alloys #3-6 few round-shaped micron-sized light particles were observed (see Fig. 2c, d, e, f). The EDS microanalysis revealed Fe, Si, and sometimes oxygen in the composition of these particles. No nucleation of primary particles enriched with Zr was found.

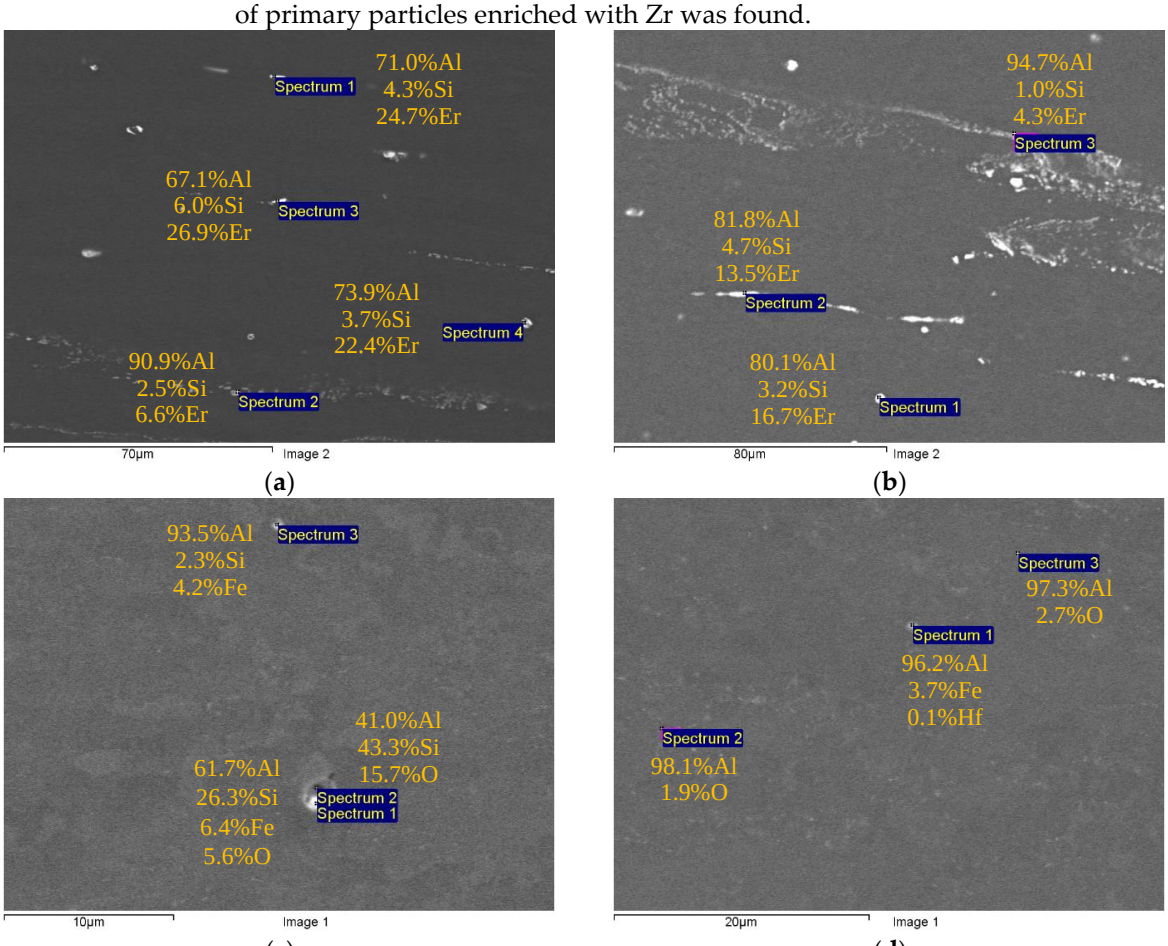

(**a**) (**b**)

(**c**) (**d**)

Preprints (www.preprints.org) | NOT PEER-REVIEWED | Posted: 22 December 2022 doi:10.20944/preprints202212.0407.v1

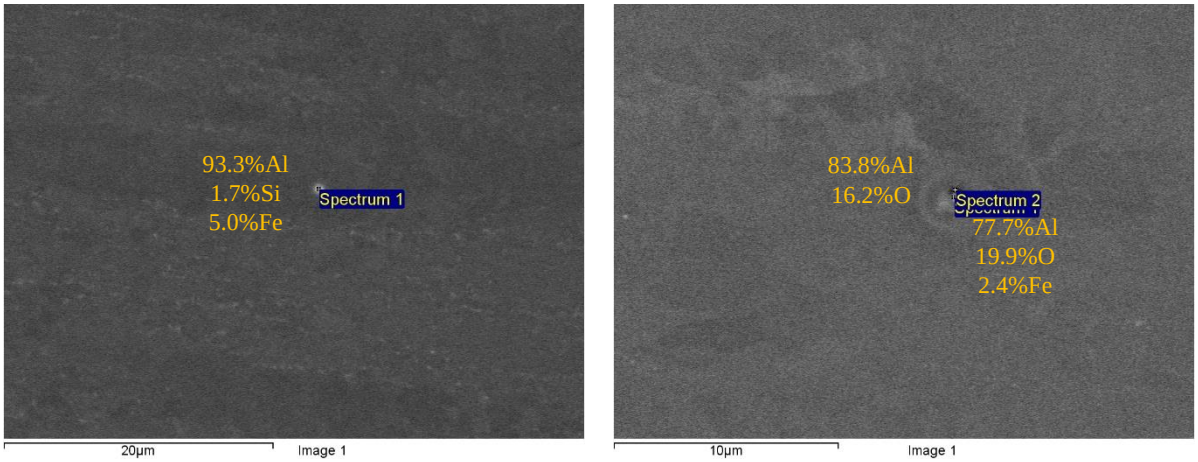

(**e**) (**f**)

Figure 3. Results EDS microanalysis of the particles in the fine-grained Alloys #1 (**a**), #2 (**b**), #3 (**c**), #4(**d**), #5 (**e**), and #6 (**f**). SEM.

The composition of the primary particles in the fine-grained alloys was similar to the one of the particles in the cast alloys (Figures 2 and 3). Note that in Alloy #4 (Al-0.25Zr-0.15Hf) the particles with insufficient amount of Hf (<0.1 wt.%) were found.

The results of investigations of the microhardness and SER of the alloys after the induction casting are presented in Table 3. Alloys #1-3 doped with silicon had the maximum microhardness. The maximum values of SER were observed in the alloys with addition of hafnium (Alloys #1, 4, 5).

Table 3. Microhardness and SER of the alloys in different states.

Characteristics	Alloy #					
	1	**2**	**3**	**4**	**5**	**6**
	After casting					
Hv, MPa	300 ± 10	295 ± 30	285 ± 10	250 ± 5	255 ± 10	250 ± 25
ϱ, μΩ·cm	3.34 ± 0.06	3.19 ± 0.03	3.20 ± 0.01	3.25 ± 0.08	3.33 ± 0.05	3.18 ± 0.05
	After severe plastic deformation					
Hv, MPa	500 ± 15	510 ± 20	465 ± 15	420 ± 15	430 ± 15	400 ± 10
ϱ, μΩ·cm	3.37 ± 0.03	3.22 ± 0.03	3.20 ± 0.02	3.28 ± 0.05	3.37 ± 0.04	3.22 ± 0.04
ϱ_{th}, μΩ·cm	3.47	3.45	3.23	3.15	3.16	3.43
f_{v0}, %	0.28	0.26	0.29	0.32	0.33	0.26
	After SPD and annealing 550 °C, 1 hr					
Hv, MPa	290 ± 5	275 ± 5	275 ± 5	245 ± 5	250 ± 5	230 ± 5
ϱ, μΩ·cm	2.97 ± 0.05	2.91 ± 0.03	2.93 ± 0.01	2.97 ± 0.05	2.94 ± 0.04	3.02 ± 0.03
d, μm	14.4 ± 0.7	18.3 ±0.8	14.4 ± 0.4	24.2 ± 0.8	15.6 ± 0.7	31.3 ± 1.2

After severe plastic deformation using ECAP and Rotary Swaging, a strongly deformed microstructure with the sizes of fragments ~0.5 μm was formed in the samples of alloys (Fig. 4). No essential differences in the microstructure of the fine-grained Alloys #1-6 were found. There are nano- and submicron-sized particles in the microstructure of the UFG alloys with increased contents of doping elements (Zr + X ≥ 0.5 wt.%) (The largest particles are marked by the dashed line in Fig. 4b).

As one can see from Table 3, the hardness of the aluminum alloys increased ~1.6 times after SPD. The maximum values of microhardness (500-510 MPa) were observed for the fine-grained Alloys #1-2 having the highest value of Hv in the cast state as well (295-300 MPa) (Table 3). The magnitudes of SER of the aluminum alloys after SPD increased insufficiently (in 0.03-0.04 μΩ·cm) but this scale of variation or SER is comparable to the uncertainty of SR measurements by eddy current method.

Preprints (www.preprints.org) | NOT PEER-REVIEWED | Posted: 22 December 2022 doi:10.20944/preprints202212.0407.v1

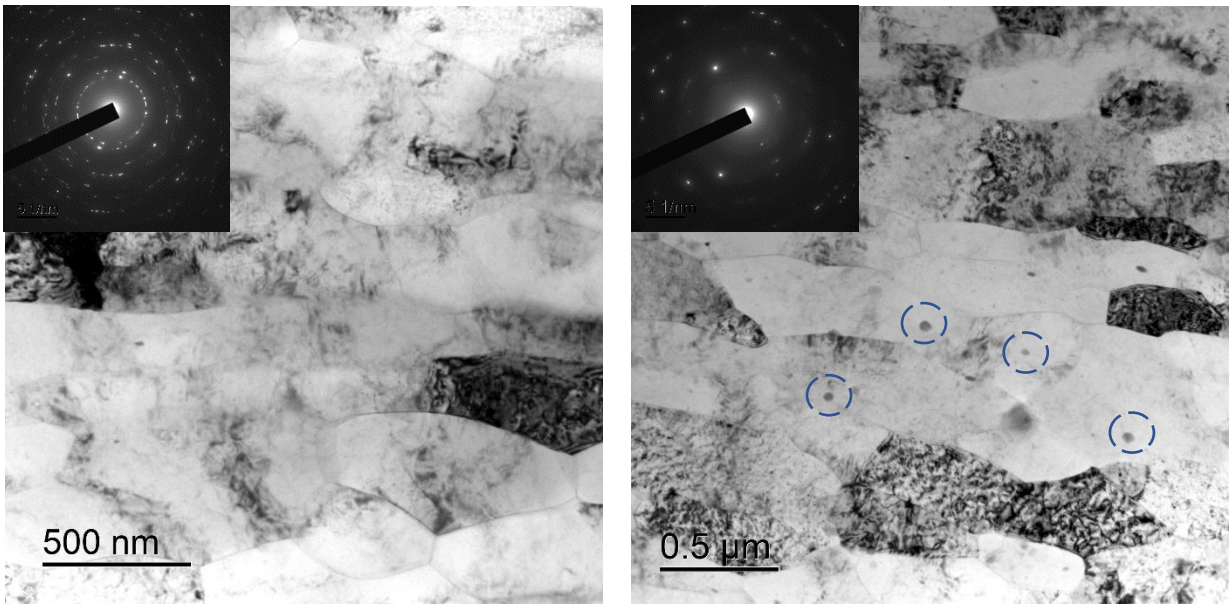

(**a**) (**b**)

Figure 4. Microstructure of the fine-grained alloys #4 (a) and #5 (b). TEM.

3.2. Effect of annealing temperature on the properties of the deformed alloys

Fig. 5 presents the dependencies of Hv and SER on the temperature of 1-hour annealing of the fine-grained alloys investigated. The analysis of the curves ρ(T) shows the magnitudes of SER to decrease with increasing annealing temperature from 200 up to 450-500 °C for all samples. Obviously, this is related to the nucleation of the particles (see [57-60, 70, 74, 97]). The Al-0.25%Zr-0.25%Hf alloy, the magnitude of SER of which 3.2 ± 0.05 μΩ·cm is achieved in after annealing at 300 °C, 1 hr is featured by the smallest intensity of SER variation in the temperature range 200-450 °C. The target level of SER of 3.0 μΩ·cm or less was achieved in all alloys after 1-hour annealing at 450 °C. An insufficient increase in SER in ~ 0.1-0.15 μΩ·cm was observed at further increasing of temperature up to 550 °C, which, in our opinion, originates from partial dissolving of large intermetallic particles Al-Fe-Si (Figures 2 and 3) and the increase in the Fe and Si contents in the solid solution. This suggestion was confirmed by investigation of temperature dependence of SER of pure aluminum, which was used for making the conductor aluminum alloys (Fig. 5a).

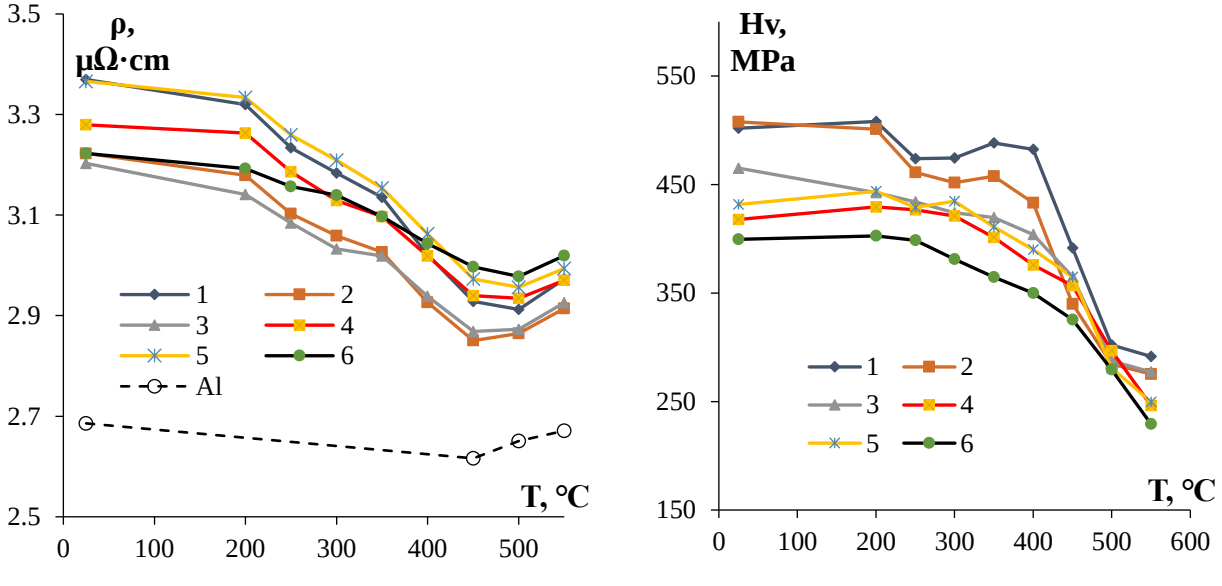

(**a**) (**b**)

Preprints (www.preprints.org) | NOT PEER-REVIEWED | Posted: 22 December 2022 doi:10.20944/preprints202212.0407.v1

Figure 5. Dependencies of SER (**a**) and microhardness (**b**) of the fine-grained aluminum Alloys #1-6 on the temperature of 1-hour annealing.

Fig. 6 presents the results of investigations of the microstructure of the alloys after the annealing at 550 °C (1 hr). The alloys have completely recrystallized microstructure. One can see in the images presented that grain growth was observed in all alloys but its intensity depends on the type and concentration of the doping elements essentially. The mean sizes of the recrystallized grains in the Alloys #1, 2, 3, and 5 were 30-40 μm whereas the grain sizes in the Alloy #4 (Fig. 6d) and in the Alloy #6 (Fig. 6f) exceed 100 μm.

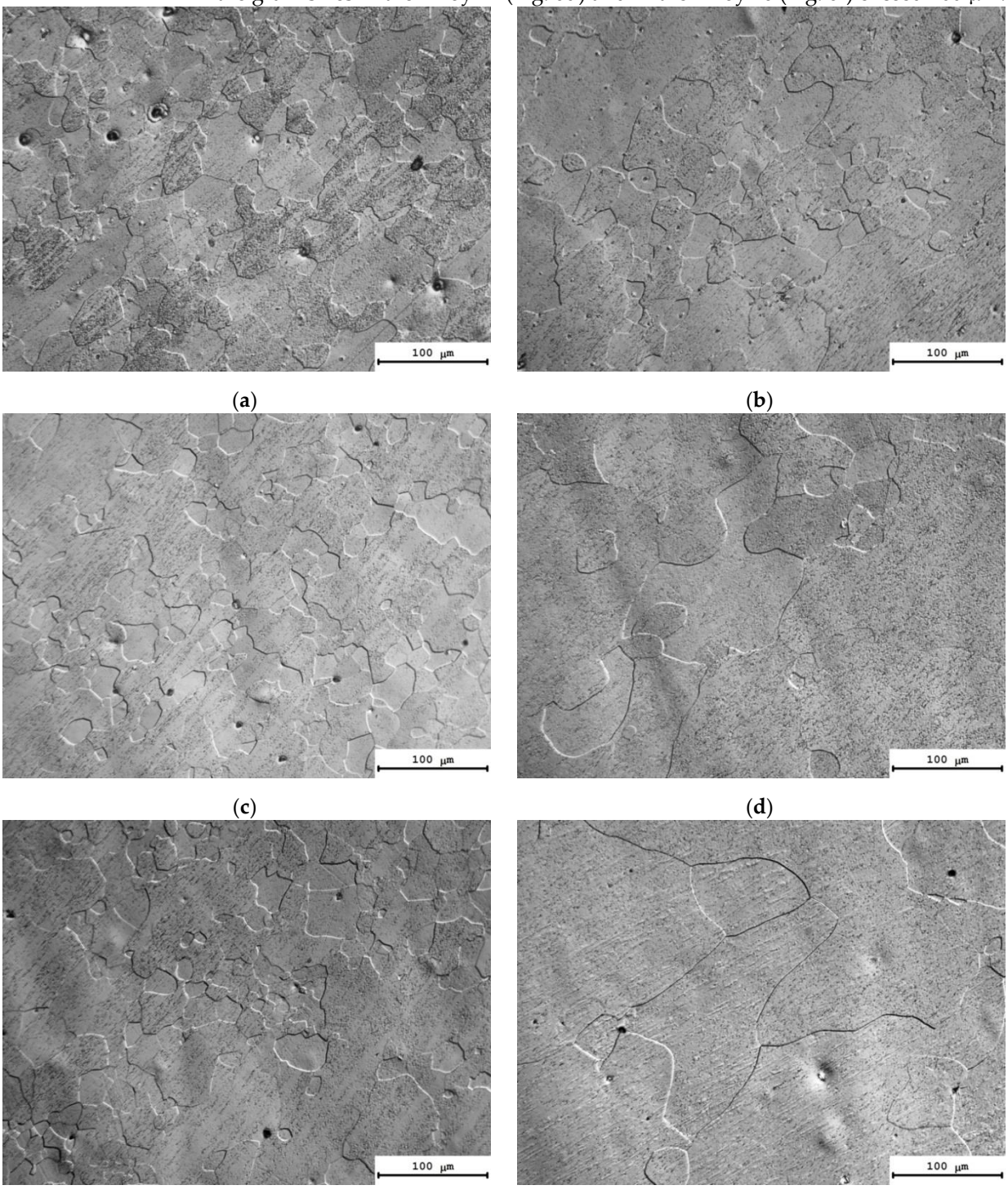

(**a**) (**b**) (**c**) (**d**) (**e**) (**f**)

Figure 6. Microstructure of the Alloys #1 (**a**), #2 (**b**), #3 (**c**), #4 (**d**), #5 (**e**), and #6 (**f**) after annealing at 550 °C, 1 hrs. Optical microscopy.

Preprints (www.preprints.org) | NOT PEER-REVIEWED | Posted: 22 December 2022 doi:10.20944/preprints202212.0407.v1

3.3. Effect of the annealing time on the properties of deformed alloys

Fig. 7 presents the dependencies of SER and microhardness of the alloys on the time of annealing at 300 °C. The choice of the isothermic annealing temperature (300 °C) was motivated by the intention to minimize the grain growth intensity resulting in a decrease in the alloy microhardness and simultaneously to ensure a high intensity of the secondary particle nucleation. (For the majority of alloys investigated, the degree of decomposition of the solid solution after 1-hour annealing at 300 °C was close to 50%.) It allows achieving the necessary (target) level of SER of the conductor aluminum alloy (3.0 μΩ·cm or less) with simultaneous ensuring its increased hardness.

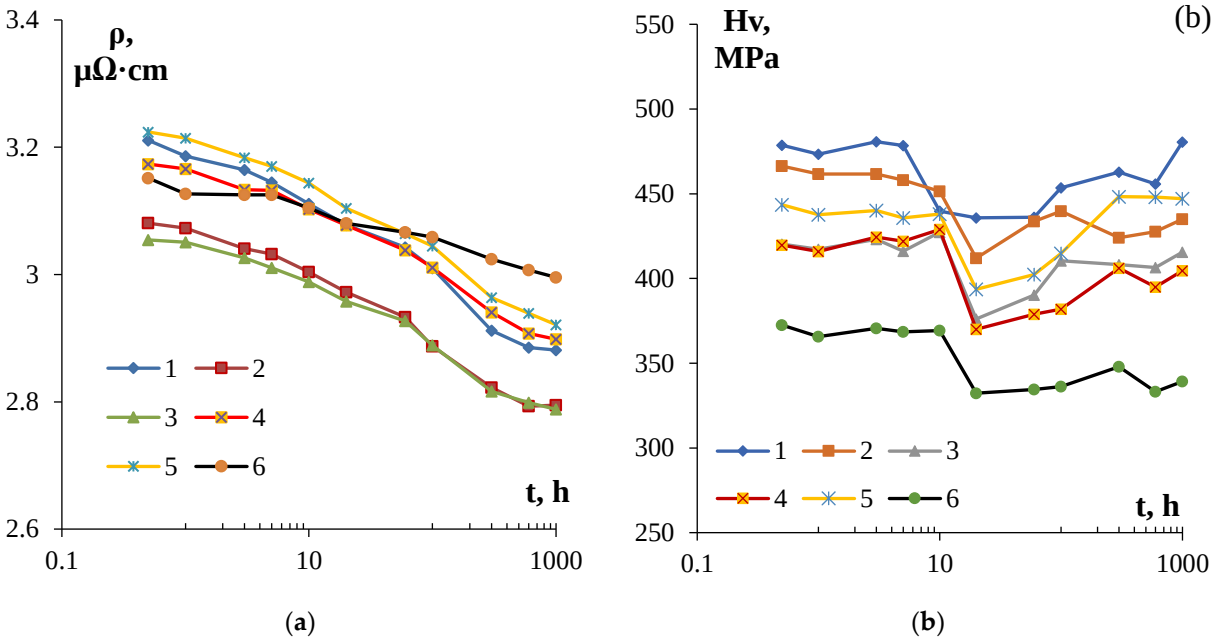

Figure 7. Dependencies of SER (**a**) and microhardness Hv (**b**) of the fine-grained aluminum alloys #1-6 on the time of annealing at 300 °C.

Analysis of the curves ρ(t) presented in Fig. 7a shows the SER of the fine-grained alloys to decrease exponentially with increasing isothermic holding time. The most intensive decreasing of SER takes place in the first 20 hrs, then the intensity of SER decreasing drops considerably. The lowest intensity of the SER decreasing (Δρ = 0.15 μΩ·cm) and, as a consequence, the highest values of SER in the annealed state (~ 3 μΩ·cm) was observed for the Alloy #6. In the fine-grained Alloy #1, the scale of decrease in SER after annealing 300 °C, 1000 hr was Δρ = 0.33 μΩ·cm.

The dependence Hv(t) had more complex character. As one can see in Fig. 7b, at small holding ties (t ≤ 20 hr), the microhardness reduced in all fine-grained samples investigated, that probably originates from the recrystallization processes. The increasing of the isothermic holding time leads to an increase in the microhardness, which originates from the nucleation of the secondary particles. The values of microhardness and SER in the annealed alloys are presented in Table 4. The maximum increase in the hardness during annealing was observed in Alloy #1; the hardness of Alloy #6 decreased continuously in the course of isothermic holding at 300 °C (Fig. 7b).

Table 4. Physical and mechanical properties, microstructure parameters and parameters of Johnson-Mehl-Avrami-Kolmogorov equation of aluminum alloys after annealing at 300 °C (1000 hrs).

Alloy #	Characteristics				Parameters of JMAK equation	
	H_v, MPa	ϱ, μΩ·cm	d, μm	f_R, %	n	m
1	480 ± 15	2.88 ± 0.04	2.0 ± 0.5	≤5	0.21	5.2
2	435 ± 10	2.79 ± 0.02	1.9 ± 0.4	≤5	0.25	4.8
3	415 ± 15	2.79 ± 0.04	2.2 ± 0.5	≤5	0.24	4.2

Preprints (www.preprints.org) | NOT PEER-REVIEWED | Posted: 22 December 2022 doi:10.20944/preprints202212.0407.v1

4	405 ± 10	2.90 ± 0.02	2.6 ± 0.6	11	0.23	2.1
5	445 ± 20	2.92 ± 0.06	2.3 ± 0.5	7	0.23	2.0
6	340 ± 10	3.00 ± 0.02	2.5 ± 0.6	12	0.20	6.9

The results of investigations of microstructure of the alloys after annealing at 300 °C, 1000 hrs are presented in Fig. 8. The calculated values of the mean grain sizes (d) and the volume fraction of the recrystallized structure (f_R) are given in Table 4. The analysis of the results of investigations shows the long isothermic annealing at 300 °C not to result in a considerable increase in the mean grain sizes. The volume fraction of the recrystallized structure was small enough and didn't exceed 10%. The highest volume fraction of the recrystallized structure (~11-12%) and large grains were observed in Alloys #4 and #6 (Table 4).

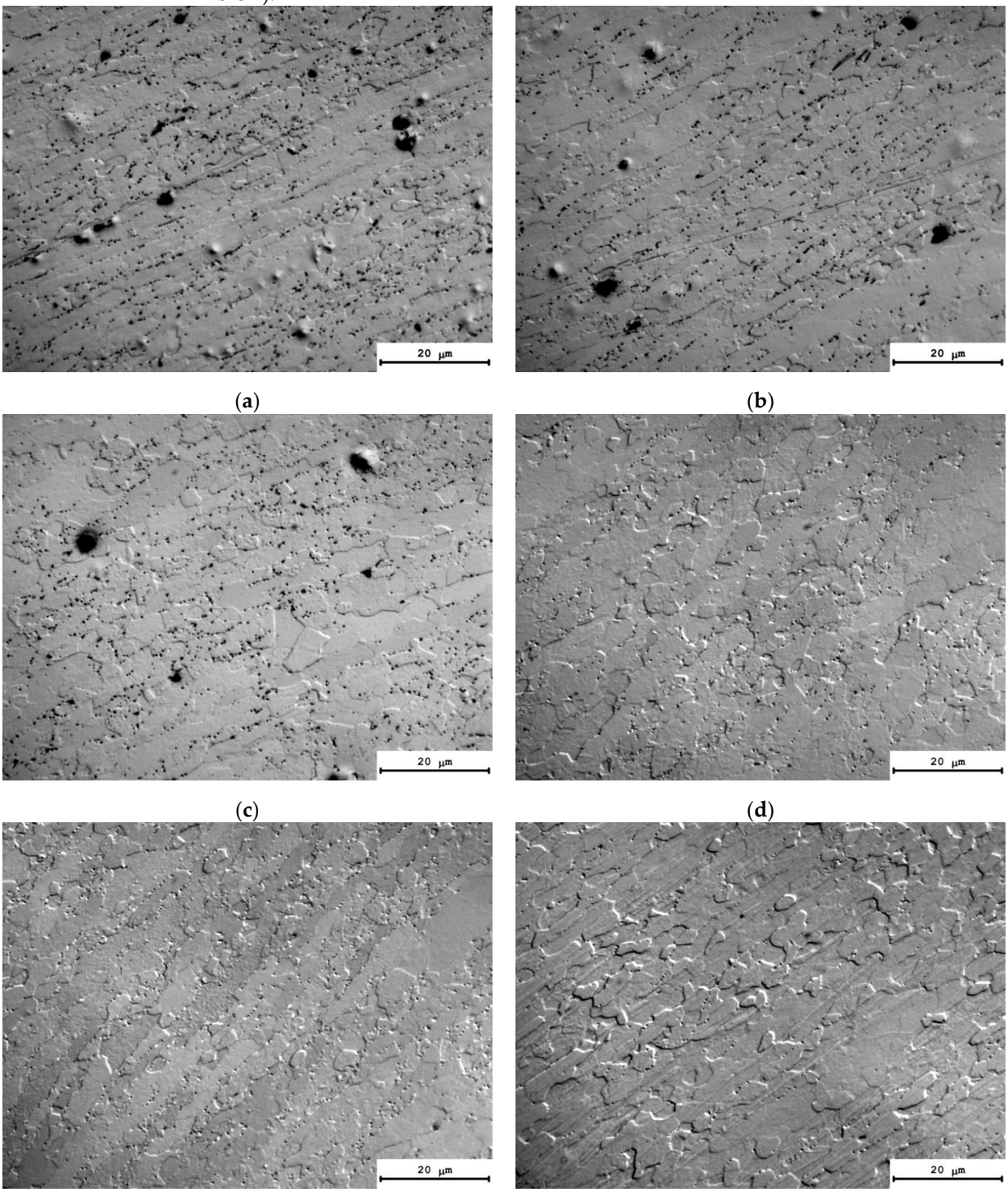

(**a**) (**b**)

(**c**) (**d**)

Preprints (www.preprints.org) | NOT PEER-REVIEWED | Posted: 22 December 2022 doi:10.20944/preprints202212.0407.v1

(**e**) (**f**)

Figure 8. Microstructure of Alloys #1 (**a**), #2 (**b**), #3 (**c**), #4 (**d**), #5 (**e**), and #6 (**f**) after annealing at 300 °C 1000 hrs. Optical microscopy.

One can see a line-wise nucleation of the micrometer- and submicron-size particles in the microstructure of partly recrystallized Alloys #1-3 (Fig. 8a-c). The particles are located preferentially at the boundaries of the recrystallized grains. No line-wise nucleated micron-sized particles were found in the microstructure of partly recrystallized Alloys #4-6 but these ones are located preferentially at the recrystallized grain boundaries as well (Fig. 8d-8f). Fig. 9 presents the dependencies of the mean grain sizes and of the volume fraction of the recrystallized structure on the annealing time. One can see from these dependencies that the increasing of the time of holding at 300 °C leads to an increasing of the mean grain sizes for all alloys. The volume fraction of the recrystallized structure also grows monotonously with increasing annealing time. The minimum values of the volume fraction of the recrystallized structure were observed for Alloys #1-3 doped with silicon.

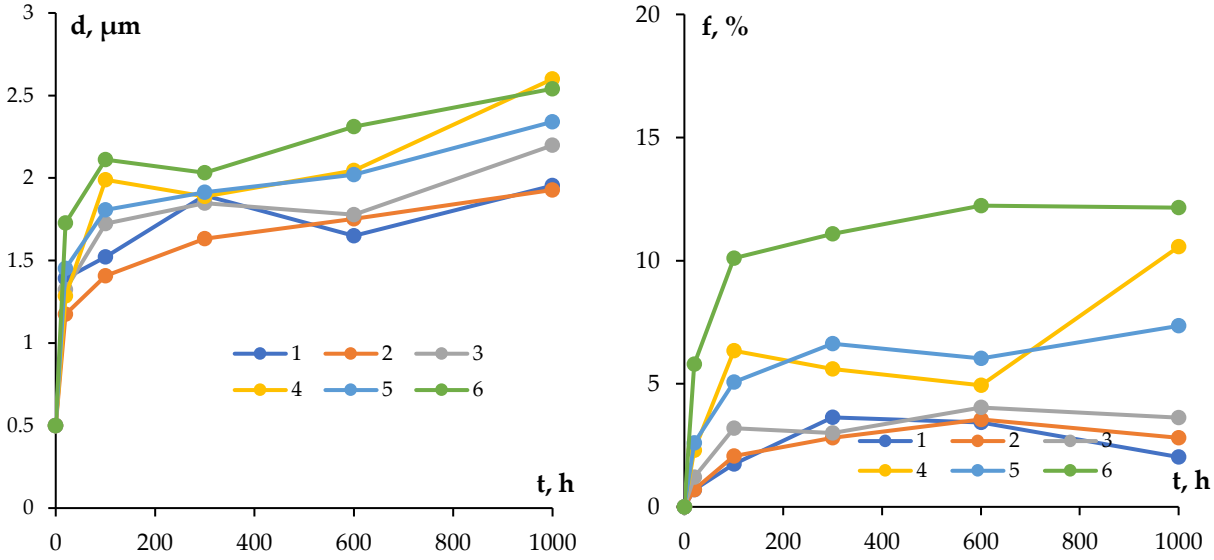

(**a**) (**b**)

Figure 9. Dependencies of the mean recrystallized grain sizes (**a**) and of the volume fraction of the recrystallized microstructures (**b**) on the time of annealing at T = 300 °C.

4. Discussion

4.1. Specific electrical resistivity. Kinetics of the particle nucleation

The theoretical values of SER (ρ_{th}) of the alloys calculated in the assumption of the additive contributions of the doping elements (Zr, Si, Er, Hf, and Nb) into the SER magnitude of aluminum are given in Table 3. This calculation can be made according to Matthiessen rule using the formula:

$$\rho_{th} = \rho_{Al} + \sum K_i C_i, \quad (1)$$

where ρ_{Al} is the SER of pure aluminum (2.7 μΩ·cm), K_i is the contribution of the i^{th} doing element into the SER of aluminum, C_i is the concentration of this doping element (in % at.). The reference data for K_i were taken from [98].

As one can see from Table 3, the theoretical values ρ_{th} for Alloys #1-3 and #6 are greater than the measured SER ones (ρ_{exp}). In our opinion, the small measured SER values are related to the partial decomposition of the solid solution in these alloys at the crystallization stage. For Alloys #4-5 of the Al-Zr-Hf system, the opposite situation was observed – the theoretical values ρ_{th} were smaller than the measured SER ones (Table 3). In further analysis, the magnitude of K_{Hf} was taken to be equal to 0.75 μΩ·cm/at.%.

Preprints (www.preprints.org) | NOT PEER-REVIEWED | Posted: 22 December 2022 doi:10.20944/preprints202212.0407.v1

Let us determine the dependence of the volume fraction of the nucleated particles on the time and temperature of annealing $f_v(t,T)$. The procedure of calculation of the volume fraction $f_v(t, T)$ based on analysis of the results of investigations of SER $\rho(t,T)$ was described in [97, 99]. According to [97], the relationship between the f_v and the variation of SER ($\Delta\rho$) can be represented in the following form: $f_v(t) = \Delta\rho(t)/K = (\varrho_0-\varrho(t))/K$ where ϱ_0 is the initial SER value (Table 3), $\varrho(t)$ is the SER after annealing with the duration t, and K is a constant describing the contribution the doping elements constituting the nucleated particles into the SER of the alloy.

The expression for the volume fraction of the secondary particles f_v can be represented in the form [99]:

$$f_v = C_r(t)/\alpha, \quad (2)$$

where α is the parameter characterizing the fraction of the impurity atoms in the particle (for the Al_3Zr particles, the magnitude of $\alpha = 1/4$ [99]) and C_r is the concentration of doping elements entering the secondary particle. The maximum volume fraction of the particles can be calculated by the formula: $f_{v0} = (C_0-C^*)/\alpha$ where C_0 is the initial concentration of the doping elements in the crystal lattice, C^* is the solubility limit of the doping elements at given temperature. To simplify the analysis, according to [99], let us assume that $C_0 >> C^*$ (in the case of solid solution of zirconium in aluminum at 300 °C, one can assume that $C^* \rightarrow 0$). The results of calculations of f_{v0} are presented in Table 3.

In this case, expression (2) can be transformed into the form:

$$f_v = f_{v_0}(\rho_0 - \rho(t))/(\rho_0 - \rho_{min}), \quad (3)$$

where ρ_{min} is the minimum value of SER, which can be accepted to be equal to the SER of pure aluminum (2.7 μΩ·cm). The dependencies $f_v(t)$ calculated according to (3) at 300 °C are presented in Fig. 10.

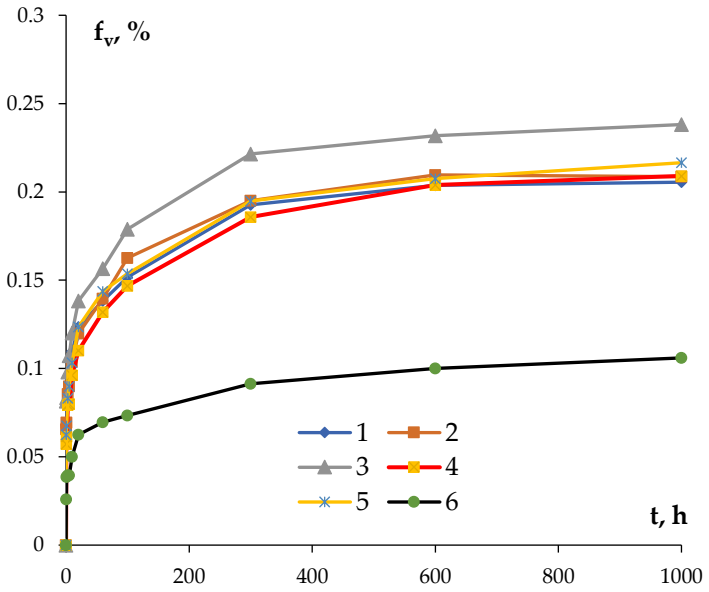

Figure 10. Dependencies of the volume fractions of the nucleated particles in aluminum alloys of the time of annealing at 300 °C.

One can see in Fig. 10 that the maximum volume fraction of the nucleated particles is characteristic for the Si-containing alloys. The minimum volume fraction of the nucleated particles was observed in Alloy #6. After holding for 600 hrs at 300 °C, the magnitudes of f_v tend to the constant values in all alloys and remain almost constant at further increasing of the annealing time.

Preprints (www.preprints.org) | NOT PEER-REVIEWED | Posted: 22 December 2022 doi:10.20944/preprints202212.0407.v1

The dependence of the volume fraction of the secondary particles on the temperature and time of annealing can be described by Johnson-Mehl-Avrami-Kolmogorov (JMAK) equation [99, 100]:

$$f_v(t, T) = f_{v0}[1-\exp(-(t/\tau)^n)], \quad (4)$$

where $\tau=\tau_0\exp(Q_R/kT)$ is the characteristic time of the diffusion process, n is the coefficient of the decomposition rate, $_0$ is the pre-exponential factor, Q_R is the effective activation energy of the particle nucleation process, and k is the Boltzmann constant.

According to [99, 100], the parameters n and Q characterize the mechanisms of nucleation of the secondary particles. At the nucleation of the coherent particles in the fine-grained aluminum alloys Al-(Sc,Zr), the relationship between the parameters *n*, *Q* and the mechanism of the solid solution decomposition can be described by the model [99]. In particular, the value of $n = 1.5$ corresponds to the case of homogeneous nucleation of the particles inside the crystal lattice, $n = 0.75$-1 – to the case of the particle nucleation at the grain boundaries or at the cores of the lattice dislocations. If at the annealing of a fine-grained material the recovery or recrystallization processes take place, the magnitude of coefficient *n* decreases down to 0.25-0.33 [99].

The values of *n* are determined from the measured curves $f_v(t,T)$ plotted in the double logarithmic axes $\ln(\ln(1-f_v/f_{v0})) - \ln(t)$ (Fig. 11). In the case if the mechanism of the solid solution decomposition doesn't change, these dependencies should comprise straight lines, the slopes of which give the magnitudes of the parameter *n* while the offset equals to $n\cdot\ln(\tau)$.

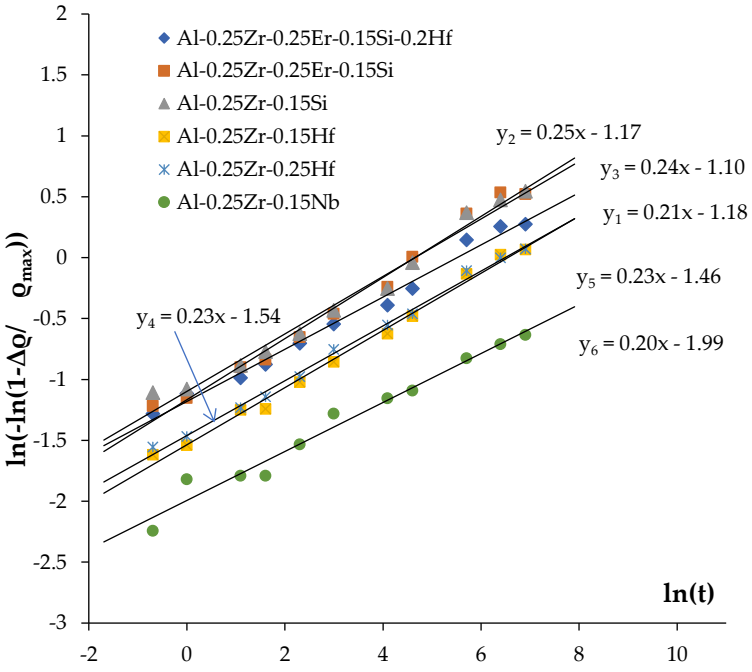

Figure 11. Analysis of the mechanisms of the secondary particle nucleation. Calculation of the coefficient *n* in JMAK equation.

As one can see in Fig. 11, the values of coefficient *n* fall into the rage 0.2-0.25 (Table 4). The confidence coefficient of the linear fit is high enough (R^2 = 0.97-099). The result obtained evidences the nucleation of secondary particles takes place preferentially at the cores of the lattice dislocations in the conditions of simultaneous recovery and recrystallization processes (see [99]). This conclusion agrees qualitatively with the results of microstructure investigations (Figures 8-9, Table. 4).

So far, one can conclude the improved thermal stability of the fine-grained microstructure of the aluminum alloy investigated toe be provided by the nucleation of secondary particles at the cores of lattice dislocations. Note that it is an important result from the

 doi:10.20944/preprints202212.0407.v1

viewpoint of applications, which allows ensuring stabilization of the nonequilibrium microstructure of the aluminum alloys at reduced annealing temperatures.

Preprints (www.preprints.org) | NOT PEER-REVIEWED | Posted: 22 December 2022 doi:10.20944/preprints202212.0407.v1

4.2. Investigation of microstructure. Particle growth during annealing

As one can see from the experimental data presented (Fig. 8), the grain growth with simultaneous nucleation and growth of the secondary particles take place in the course of annealing (Fig. 10). The particles nucleating during annealing prevent the migration of grain boundaries and provide the increased thermal stability of the nonequilibrium microstructure of the fine-grained aluminum alloys. According to [101], the relationship between the particle size R, the volume fraction of these ones f_v, and the mean size of the recrystallized grains d is determined by Zener equation:

$$d_Z = \alpha_1 R/f_v, \quad (6)$$

where α_1 is a coefficient depending on the particle shape (α = 4/3 for the spherical particles). It follows from Equation (6) that one has to ensure a high intensity of nucleation and low growth rate of the particles in order to provide an increased stability of microstructure.

Comparing the results of the metallographic investigations, on the base of which *d* was determined (Fig. 8a) and the ones of SER investigations allowing determining f_v (Fig. 10), let us calculate the size of nucleated secondary particles R in the aluminum alloys. The curves R(t) at T = 300 °C are presented in Fig. 12.

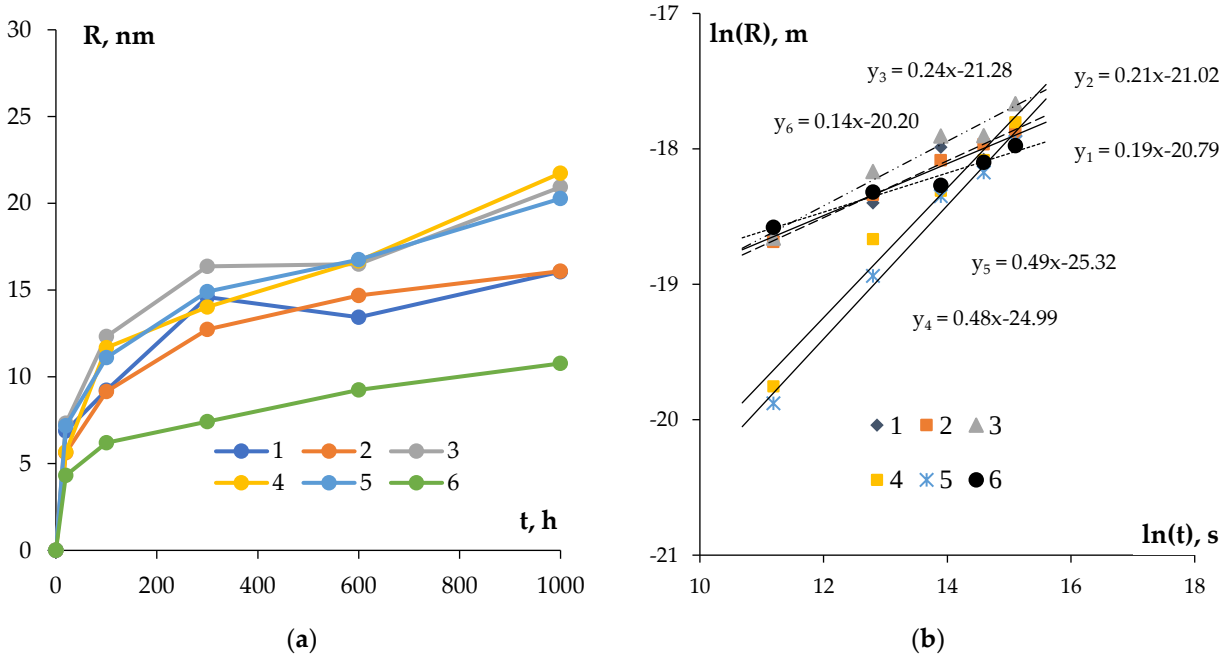

Figure 12. Dependencies of the particle sizes in the aluminum alloys on the time of annealing at T = 300 °C in the linear (a) and logarithmic (b) axes.

One can see in Fig. 12a a monotonous increase in the mean particle sizes in the course of annealing at T = 300 °C to be observed in all alloys. All alloys had approximately growth rate of the secondary particles except Alloys #6 containing Nb in its chemical composition. In average, the particle sizes in the alloys increased 2-3 times from the initial values after 1000 hrs of annealing.

The growth of the secondary particles is known to be described by the equation [101, 102]:

$$R^m - R_0^m = \xi D_0 t \exp(-Q_2/kT), \quad (5)$$

where R and R_0 are the current and initial radii of the secondary particle, respectively, *m* is the growth rare coefficient, Q_2 is the activation energy of the secondary particle growth process, ξ is a numerical coefficient, and D_0 is the pre-exponential factor in the diffusion equation. Using Equation (5), one can estimate the magnitude of coefficient *m*, which depends on the dominating diffusion mechanism limiting the growth intensity of the

 doi:10.20944/preprints202212.0407.v1

secondary particles [100, 102]. According to (5), the quantity 1/*m* corresponds to the slope of the curve R(t) in the logarithmic axes lnR – lnt.

Note that the magnitude of the coefficient m determines the dominating mechanism of the particle growth [100, 102]. In the case of particle growth inside the crystal lattice of aluminum $m = 3$, at the grain boundaries and at the dislocation cores (in the case of a stale microstructure) – $m = 4$ [100, 102]. In the case if the microstructure of the aluminum alloy is unstable and the secondary particles nucleate at the cores of the lattice dislocations, the magnitude of coefficient *m* varies from 6 to 12 [102].

The analysis of the data presented in Fig. 12b shows the minimum values of coefficient *n* to be observed for Alloys #4-5 of the system Al-0.25%Zr-Hf (Table 4). The result obtained evidences the $Al_3(Zr,Hf)$ particles, which nucleated first at the cores of the lattice dislocations (see Subsection 4.1) to grow further via volume diffusion. It can occur because of simultaneous decrease in the density of the lattice dislocations as well as because of a large (as compared to Zr) intensity of diffusion of the Hf atoms in the crystal lattice of aluminum at 300 °C.

The fine-grained Nb-containing Alloy #6 has the highest value of the coefficient $n = 6.9$ among the alloys investigated (Table 4). The result obtained evidences the rates of nucleation and growth of the $Al_3(Zr,Nb)$ particles in this fine-grained alloy to be limited by the intensity of diffusion in the dislocation cores.

For the Si-containing fine-grained Alloys #1-3, the magnitude of the coefficient $n \sim 4$-5 that probably points to the growth of the secondary particles at the grain boundaries (see [102]). This conclusion agrees well with rapid nucleation and growth of the secondary particles in the Si-containing aluminum alloys described above.

Summarizing the results of the analysis performed, one can conclude the nucleation of the secondary particles in the alloys investigated to take place at the cores of dislocations while the mechanism of their further growth depends on the type of the relationship of the volume, dislocation, and grain boundary diffusion coefficients of the doping elements in aluminum at given annealing temperature as well as on the character of their the spatial distribution (the uniform distribution inside the material bulk or formation of the grain boundary segregations).

4.3. Optimization of microhardness and SER

Fig. 13 shows the dependencies of the electrical conductivity (in the IACS units) on the microhardness for the aluminum alloys investigated. This chart is a convenient tool for optimizing the thermal processing regimes of the aluminum alloys Al-0.25Zr with different compositions of the doping additives allowing selecting the optimal relation between the hardness and SER.

Preprints (www.preprints.org) | NOT PEER-REVIEWED | Posted: 22 December 2022 doi:10.20944/preprints202212.0407.v1

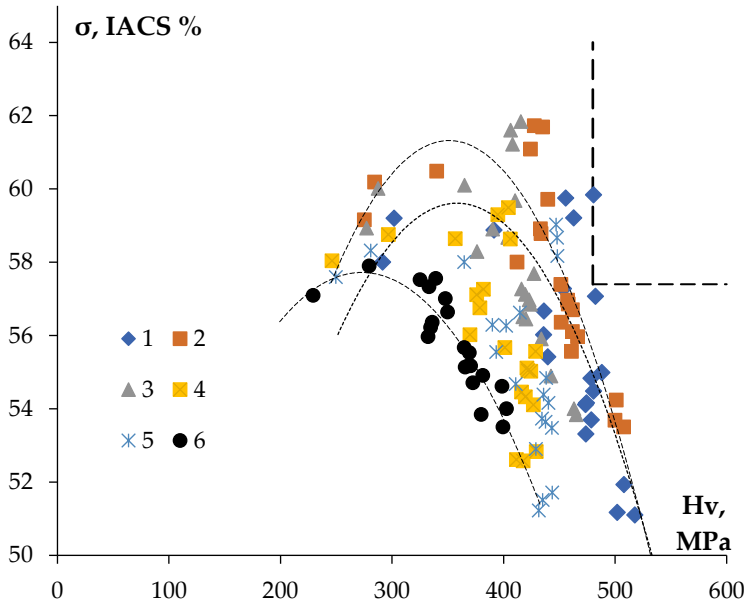

Figure 13. Dependence of the electrical conductivity (IACS) on the microhardness for the fine-grained aluminum alloys Al-0.25Zr-(Si, Er, Hf, Nb).

As it has been already mentioned above, the target value of SER, which is necessary to achieve in the conductor aluminum alloy is 3.0 μΩ·cm that corresponds to 57.4 IACS. The minim value of the ultimate strength for new conductor alloy should be not less than the one of alloy 01417 ($\sigma_b \geq 160$ MPa). For the fine wires from the aluminum alloys, the microhardness H_v is related to the magnitude of the ultimate strength by the relation $H_v = \beta \cdot \sigma_b$ where β is a numerical coefficient depending of the structure state of the alloys [57, 58]. For the fine-grained conductor alloys β = 1.43, for the annealed aluminum alloys β = 3.45 [57, 58]. The aluminum alloys investigated were in partly recrystallized state (Table 4) and the magnitude of the coefficient β for these ones can be accepted to be equal to ~3. So far, the minimum value of microhardness for the aluminum alloys investigated should be Hv ≥ 480 MPa. The ranges of parameters (the microhardness and the electrical conductivity), which the material of a fine wire should fall into is shown by a dashed line in the upper right corner of the chart "electrical conductivity – microhardness" in Fig. 13.

The characteristics of Alloy #1 after annealing at 300 °C, 1000 hrs (59.8%IACS, Hv = 480 ± 15 MPa) satisfy to this range of the values. This alloy has a uniform fine-grained structure with the grain sizes ~ 2 μm (Table 4, Fig. 8a). Also, the characteristics of Alloy #1 after annealing at 400 °C, 1 hr (57.1%IACS, H_v = 482 MPa) are the closest to this range of parameters.

In our opinion, to improve the combination of properties of Alloy #1 further, one should optimize its chemical composition as well as optimize the casting regimes for Alloy #1 – as one can see from Table 2, the formation of large primary particles took place during the crystallization of Alloy #1. These particles didn't contribute to the strength and electrical conductivity of the alloy essentially. According to the results of the EDS microanalysis (Fig. 2a, 3a), there are considerable concentrations of silicon (Si) and erbium (Er) in the composition of the primary particles. No traces of Zr and Hf were found in the composition of the primary particles (Fig. 2a, 3a). In our opinion, the result obtained allows concluding the reduction of Si and Er concentrations would allow avoiding the formation of large primary particles during crystallization. The large primary particles can grow via coalescence at further annealing and reduce the intensity of nucleation of the nanoparticles providing the increased strength and stability of the fine-grained aluminum alloy. Besides, the large primary particles can lead to failure of a fine wire during fabrication by rolling in rolls or drawing.

5. Conclusions

1. The features of nucleation of the $Al_3(Zr,X)$ secondary particles during the annealing of fine-grained Al-0.25%Zr alloys with addition of Er, Si, Hf, and Nb were investigated. All alloys were found to preserve their fine-grained structure during annealing at 300 °C for 1000 hrs. The volume fraction of the recrystallized microstructure was small enough and didn't exceed 10%, the mean grain sizes were close to 2-2.5 μm. The mechanisms of nucleation of the secondary particles were identified by the analysis of the dependencies of the SER on the annealing time using Jones-Mehl-Avrami-Kolmogorov (JMAK). The magnitude of the coefficient *n* in JMAK equation for the alloys investigated was shown to be close to 0.20-0.24 that corresponds to the case of nucleation of the secondary particles at the cores of dislocation in the conditions of simultaneous recovery and recrystallization processes. Using Zener equation, the dependence of the secondary particle sizes on the annealing time was determined. The secondary particle growth mechanism was shown to depend on the type of the relationship between the diffusion coefficients for the volume, dislocation, and grain boundary diffusion of the doping elements in aluminum at given annealing temperature as well as on the character of their spatial distribution (uniform distribution in the volume of material, formation of grain boundary segregations). In the Hf- and Si-containing alloys, the secondary particle growth is controlled by the volume diffusion while in the Nb-containing alloy – by diffusion via the cores of lattice dislocations.

2. The effect of small (0.15-0.25%) additives of Er, Si, Hf, and Nb on the thermal stability of microstructure, SER and microhardness of the conductor aluminum alloy Al-0.25%Zr was investigated. The Al-0.25%Zr-0.25%Er-0.20%Hf-0.15%Si alloy subjected to annealing at 300 °C, 1000 hrs has the optimal combination of the microhardness and SER. The alloy after annealing has a uniform fine-grained structure; the mean grain size was ~ 2 μm, the SER was 59.8%IACS, Hv = 480 ± 15 MPa. The high characteristics of this alloy (57.1%IACS, Hv = 482 MPa) can be ensured by annealing at 400 °C, 1 hr. The characteristics of the novel alloy allow its efficient application in the aircraft building industry to replace the commercial eutectic alloys with increased contents of REEs and TMs.

Author Contributions: Conceptualization, A.N. and V.C.; methodology, A.N.; validation, A.N. and G.N.; formal analysis, A.N. and V.C.; investigation, G.N., V. K., A.B., N.T.; resources, A.N. and V.C.; data curation, A.N. and G.N.; writing—original draft preparation, A.N. and G.N.; writing—review and editing, A.N. and V.C.; visualization, A.N.; supervision, A.N. and V.C.; project administration, A.N.; funding acquisition, A.N. All authors have read and agreed to the published version of the manuscript.

Funding: This research was funded by Russian Science Foundation, grant number 20-19-00672. The investigations of the microstructure of the alloys by TEM were carried out using the instrumentation of the Center Collective Use "Materials Science and Metallurgy" (National University of Science and Technology "MISIS") supported by Ministry of Science and Higher Education of the Russian Federation (grant No. 075-15-2021-696).

Institutional Review Board Statement: Not applicable.

Informed Consent Statement: Not applicable.

Data Availability Statement: Not applicable.

Conflicts of Interest: The authors declare no conflict of interest.

References

1. Sasaki, T.T.; Morris, R.A.; Thompson, G.B.; Syarif, Y.; Fox, D. Formation of ultra-fine copper grains in copper clad aluminum wire. *Scr. Mater.* **2010**, *63*, 488-491. doi:10.1016/j.scriptamat.2010.05.010
2. Ahmed, N. Extrusion of copper clad aluminum wire. *J. Mech. Working Tech.* **1978**, *2*, 19-32. doi:10.1016/0378-3804(78)90012-8
3. Yang, C.; Masquellier, N.; Gandiolle, C.; Sauvage, X. Multifunctional properties of composition graded Al wires. *Scr. Mater.* **2020**, *189*, 21–24. doi:10.1016/j.scriptamat.2020.07.052
4. Chen, X.; Tang, X.; Wang, Z.; Hui, X.; Li, M.; Wang, Y. Manufacturing process and microstructure of copper-coated aluminum wires, *Int. J. Minerals, Metallurgy, and Mater.* **2015**, *22*, 190-196. doi:10.1007/s12613-015-1060-8

5. Li, Y.; Hu, A.; Fu, Y.; Liu, S.; Shen, W.; Hu, H.; Nie, X. Al alloys and casting processes for induction motor applications in battery-powered electric vehicles: A review. *Metals* **2022**, *12*, 216. doi:10.3390/met12020216
6. Hou, J.P.; Li, R.; Wang, Q.; Yu, H.Y.; Zhang, Z.J.; Chen, Q.Y.; Ma, H.; Wu, X.M.; Li, X.W.; Zhang, Z.F. Breaking the trade-off relation of strength and electrical conductivity in pure Al wire by controlling texture and grain boundary. *J. Alloys Compd.* **2018**, *769*, 96-109. doi:10.1016/j.jallcom.2018.07.358
7. Pourbashiri, M.; Poletti, C.; Sedighi, M.; Sommitsch, C. Strengthening mechanisms of Al wires processed by equal channel angular torsion drawing. *Mater. Sci. Techn.* **2020**, *36*, 65-82. doi:10.1080/02670836.2019.1682788
8. Li, R.; Liu, H.; Ma, H.; Hou, J.; Qian, L.; Wang, Q.; Li, X.; Zhang, Z. Role of multi-scale microstructure in the degradation of Al wire for power transmission. *Appl. Sci.* **2020**, *10*, 2234. doi:10.3390/app10072234
9. Koprowski, P.; Lech-Grega, M.; Wodziński, Ł.; Augustyn, B.; Boczkal, S.; Ożóg, M.; Uliasz, P.; Żelechowski, J.; Szymański, W. The effect of low content additives on strength, resistivity and microstructural changes in wire drawing of 1xxx series aluminium alloys for electrical purposes. *Mater. Today Comm.* **2020**, *24*, 101039. doi:10.1016/j.mtcomm.2020.101039
10. Wang, Y.; Zhu, L.; Niu, G.; Mao, J. Conductive Al alloys: the contradiction between strength and electrical conductivity. *Adv. Eng. Mater*. **2021**, *23*, 2001249. doi:10.1002/adem.202001249
11. Hou, J.P.; Li, R.; Wang, Q.; Yu, H.Y.; Zhang, Z.J.; Chen, Q.Y.; Ma, H.; Wu, X.M.; Li, X.W.; Zhang, Z.F. Three principles for preparing Al wire with high strength and high electrical conductivity. *J. Mater. Sci. Tech.* **2019**, *35*, 742-751. doi:10.1016/j.jmst.2018.11.013
12. Mavlyutov, A.M.; Bondarenko, A.S.; Murashkin, M.Yu.; Boltnynjuk, E.V.; Valiev, R.Z.; Orlova, T.S. Effect of annealing and electrical resistivity of nanostructured SPD aluminium. *J. Alloys Compd.* **2017**, *698*, 539-546. doi:10.1016/j.jallcom.2016.12.240
13. Hou, J.P.; Chen Q.Y.; Wang, Q.; Yu, H.Y.; Zhang, Z.J.; Li, R.; Li, X.W.; Zhang, Z.F. Effects of annealing treatment on the microstructure evolution and the strength degradation behavior of the commercially pure Al conductor. *Mater. Sci. Eng. A* **2017**, *707*, 511-517. doi:10.1016/j.msea.2017.09.075
14. Orlova, T.S.; Mavlyutov, A.M.; Bondarenko, A.S.; Kasatkin, I.A.; Murashkin, M.Yu.; Valiev, R.Z. Influence of grain boundary state on electrical resistivity of ultrafine grained aluminium. *Phil. Mag.* **2016**, *96*, 2429-2444. doi:10.1080/14786435.2016.1204022
15. Fereshteh-Saniee, F.; Asgari, M.; Fakhar, N. Specialized mechanical properties of pure aluminum by using non-equal channel angular pressing for developing its electrical applications. *Appl. Phys. A* **2016**, *122*, 779. doi:10.1007/s00339-016-0305-3
16. Murashkin, M.Yu.; Sabirov, I.; Sauvage, X.; Valiev, R.Z. Nanostructured Al and Cu alloys with superior strength and electrical conductivity. *J. Mater. Sci.* **2016**, *51*, 33-49. doi:10.1007/s10853-015-9354-9
17. Matveev, Yu.A.; Gavrilova, V.P.; Baranov, V.V. Light conducting materials for aircraft wires. *Cables Wires* **2006**, *5*, 22–23. (in Russian). https://www.elibrary.ru/item.asp?id=9299129
18. Sidelnikov, S.B.; Voroshilov, D.S.; Motkov, M.M.; Timofeev, V.N.; Konstantinov, I.L.; Doyzhenko, N.N.; Lopatina, E.S.; Bespalov, V.M.; Sokolov, R.E.; Mansurov, Y.N.; et al. Investigation structure and properties of wire from the alloy of Al-REM system obtained with the application of casting in the electromagnetic mold, combined rolling-extrusion, and drawing. *Int. J. Adv. Manuf. Technol.* **2021**, *114*, 2633–2649. doi:10.1007/s00170-021-07054-x
19. Korotkova, N.O.; Belov, N.A.; Timofeef, V.N.; Motkov, M.M.; Cherkasov, S.O. Influence of heat treatment on the structure and properties of an Al-7%REM conductive aluminum alloy casted in an electromagnetic crystallizer. *Phys. Met. Metallogr.* **2020**, *121*, 173–179. doi:10.1134/S0031918X2002009X
20. Sidelnikov, S.B.; Voroshilov, D.S.; Motkov, M.M.; Timofeev, V.N.; Konstantinov, I.L.; Doyzhenko, N.N.; Lopatina, E.S.; Bespalov, V.M.; Sokolov, R.E.; Mansurov, Y.N.; et al. Investigation structure and properties of wire from the alloy of Al-REM system obtained with the application of casting in the electromagnetic mold, combined rolling-extrusion, and drawing. *Int. J. Adv. Manuf. Technol.* **2021**, *114*, 2633–2649. doi:10.1007/s00170-021-07054-x
21. Teleshov, V.V.; Zakharov, V.V.; Zapolskaya, V.V. Development of aluminium alloys for high-temperature wires with enhanced strength and high specific electrical conduction. *Light Alloy. Technol.* **2018**, *1*, 15–26. (in Russian)
22. Mogucheva, A.A.; Zyabkin, D.V.; Kaibyshev, R.O. Effect of annealing on the structure and properties of aluminum alloy Al-8%MM. *Met. Sci. Heat Treat.* **2012**, *53*, 450–454. doi:10.1007/s11041-012-9414-6
23. [33] Murashkin, M.Yu.; Sabirov, I.; Medvedev, A.E.; Enikeev, N.A.; Lefebvre, W.; Valiev, R.Z.; Sauvage, X. Mechanical and electrical properties of an ultrafine grained Al-8.5wt.%RE (RE = 5.4wt.%Ce, 3.1wt.%La) alloy processed by severe plastic deformation. *Mater. Des.* **2016**, *90*, 433–442. doi:10.1016/j.matdes.2015.10.163
24. Medvedev, A.E.; Murashkin, M.Yu.; Enikeev, N.A.; Valiev, R.Z.; Hodgson, P.D.; Lapovok, R. Enhancement of mechanical and electrical properties of Al-Re alloys by optimizing rare-earth concentration and thermo-mechanical treatment. *J. Alloys Compd.* **2018**, *745*, 696–704. doi:10.1016/j.jallcom.2018.02.247
25. Wang, W.; Pan, Q.; Lin, G.; Wang, X.; Sun, Y.; Wang, X.; Ye, J.; Sun, Y.; Yu, Y.; Jiang, F.; Li, J.; Liu, Y. Microstructure and properties of novel Al-Ce-Sc, Al-Ce-Y, Al-Ce-Zr and Al-Ce-Sc-Y alloy conductors processed by die casting, hot extrusion and cold drawing. *J. Mater. Sci. Technol.* **2020**, *58*, 155–170. doi:10.1016/j.jmst.2020.03.073
26. Medvedev, A.E.; Murashkin, M.Y.; Enikeev, N.A.; Bikhmukhametov, I.; Valiev, R.Z.; Hodgson, P.D.; Lapovok, R. Effect of eutectic Al-(Ce,La) phase morphology on microstructure, mechanical properties, electrical conductivity and heat resistance of Al-4.5(Ce,La) alloy after SPD and subsequent annealing. *J. Alloys Compd.* **2019**, *796*, 321-330. doi:10.1016/j.jallcom.2019.05.006

27. Zhang, Y.; Wei, F.; Mao, J.; Niu, G. The difference of La and Ce as additives of electrical conductivity aluminum alloys. *Mater. Charact.* **2019**, *158*, 109963. doi:10.1016/j.matchar.2019.109963
28. Khangholi, S.N.; Javiani, M.; Maltais, A.; Chen, X.G. Review on recent progress in Al-Mg-Si 6xxx conductor alloys. *J. Mater. Res.* **2022**, *37*, 670-691. doi:10.1557/s43578-022-00488-3
29. Medvedev, A.; Arutyunyan, A.; Lomakin, I.; Bondarenko, A.; Kazykhanov, V.; Enikeev, N.; Raab, G.; Murashkin, M. Fatigue properties of ultra-fine grained Al-Mg-Si wires with enhanced mechanical strength and electrical conductivity. *Metals* **2018**, *8*, 1034. doi:10.3390/met8121034
30. Yuan, W.; Liang, Z. Effect of Zr addition on properties of Al-Mg-Si aluminum alloy used for all aluminum alloy conductor. *Mater. Des.* **2011**, *32*, 4195-4200. doi:10.1016/j.matdes.2011.04.034
31. Jiang, S.; Wang, R. Grain size-dependent Mg/Si ratio effect on the microstructure and mechanical/electrical properties of Al-Mg-Si alloys. *J. Mater. Sci. Tecnh.* **2019**, *35*, 1354-1363. doi:10.1016/j.jmst.2019.03.011
32. Zhao, N.; Ban, C.; Wang, H.; Cui, J. Optimized combination of strength and electrical conductivity of Al-Mg-Si alloy processed by ECAP with two-step temperature. *Materials* **2020**, *13*, 1511. doi:10.3390/ma13071511
33. Han, Y.; Shao, D.; Chen, B.A.; Peng, Z.; Zhu, Z.X.; Zhang, Q.; Chen, X.; Liu, G.; Li, X.M. Effect of Mg/Si ratio on the microstructure and hardness-conductivity relationship of ultrafine-grained Al-Mg-Si alloys. *J. Mater. Sci.* **2017**, *52*, 4445-4459. doi:10.1007/s10853-016-0691-0
34. Zhao, Q.; Qian, Z.; Cui, X.; Wu, Y.; Liu, X. Influences of Fe, Si and homogenization on electrical conductivity and mechanical properties of dilute Al-Mg-Si alloy. *J. Alloys Compd.* **2016**, *666*, 50-57. doi:10.1016/j.jallcom.2016.01.110
35. Liu, C.H.; Chen, J.; Lai, Y.X.; Zhu, D.H.; Gu, Y.; Chen, J.H. Enhanced electrical conductivity and strength in Al alloys by modification of conventional thermos-mechanical process. *Mater. Des.* **2015**, *87*, 1-5. doi:10.1016/j.matdes.2015.07.133
36. Murashkin, M.Yu.; Sabirov, I.; Kazykhanov, V.U.; Bobruk, E.V.; Dubravina, A.A.; Valiev, R.Z. Enhanced mechanical properties and electrical conductivity in ultrafine-grained Al alloy processed via ECAP-PC. *J. Mater. Sci.* **2013**, *48*, 4501-4509. doi:10.1007/s10853-013-7279-8
37. Mikhaylovskaya, A.V.; Chayoumabadi, M.E.; Mochugovskiy, A.G. Superplasticity and mechanical properties of Al-Mg-Si alloy doped with eutectic-forming Ni and Fe, and dispesoid-forming Sc and Zr elements. *Mater. Sci. Eng. A* **2021**, *817*, 141319. doi:10.1016/j.msea.2021.141319
38. Bobruk, E.V.; Dolzhenko, P.D.; Murashkin, M.Yu.; Valiev, R.Z.; Enikeev, N.A. The microstructure and strength of UFG 6060 alloy after superplastic deformation at a lower homologous temperature. *Materials* **2022**, *15*, 6983. 10.3390/ma15196983
39. Murashkin, M.; Medvedev, A.; Kazykhanov, V.; Krokhin, A.; Raab, G.; Enikeev, N.; Valev, R.Z. Enhanced mechanical properties and electrical conductivity in ultrafine-grained Al 6101 alloy processed via ECAP-Conform. *Metals* **2015**, *5*, 2148-2164. doi:10.3390/met5042148
40. Khangholi, S.N.; Javiani, M.; Maltais, A.; Chen, X.G. Optimization of mechanical properties and electrical conductivity in Al-Mg-Si 6201 alloys with different Mg/Si ratios. *J. Mater. Res.* **2020**, *35*, 2765-2776. doi:10.1557/jmr.2020.249
41. Alshwawreh, N.; Alhamarneh, B.; Altwarah, Q.; Quandour, S.; Barghout, S.; Ayasrah, O. Electrical resistivity and tensile strength relationship in heat-treated all aluminum alloy wire conductors // *Mater.* **2021**, *14*, 5738. doi:10.3390/ma14195738
42. Zhao, Q.; Quan, Z.; Cui, X.; Wu, Y.; Liu, X. Optimizing microstructures of dilute Al-Fe-Si alloys designed with enhanced electrical conductivity and tensile strength. *J. Alloys Compd.* **2015**, *650*, 768-776. doi:10.1016/j.jallcom.2015.08.052
43. Hou, J.P.; Li, R.; Wang, Q.; Yu, H.Y.; Zhang, Z.J.; Chen, Q.Y.; Ma, H.; Li, X.W.; Zhang, Z.H. Origin of abnormal strength-electrical conductivity relation for an Al-Fe alloy wire. *Materialia* **2019**, *7*, 100403. doi:10.1016/j.mtla.2019.100403
44. Medvedev, A.E.; Murashkin, M.Y.; Enikeev, N.A.; Valev, R.Z.; Hodgson, P.D.; Lapovok. R. Optimizing of strength-electrical conductivity properties in Al-2Fe alloy by severe plastic deformation and heat treatment. *Adv. Eng. Mater.* **2018**, *20*, 1700867. doi:10.1002/adem.201700867
45. Booth-Morrison, C.; Dunand, D.C.; Seidman, D.N. Coarsening resistance at 400 °C pf precipitation-strengthened Al-Zr-Sc-Er alloys. *Acta Mater.* **2011**, *59*, 7029-7042. doi:10.1016/j.actamat.2011.07.057
46. Pozdniakov, A.V.; Barkov, R.Yu.; Amer, S.M.; Levchenko, V.S.; Kotov, A.D.; Mikhaylovskaya, A.V. Microstructure, mechanical properties and superplasticity of the Al-Cu-Y-Zr alloy. *Mater. Sci. Eng. A* **2019**, *758*, 28-35. doi:10.1016/j.msea.2019.04.118
47. Gorlov, L.E.; Loginova, I.S.; Glavatskikh, M.V.; Barkov, R.Yu.; Pozdniakov, A.V. Novel precipitation strengthened Al-Y-Sc-Er alloy with high mechanical properties, ductility and electrical conductivity produced by different thermomechanical treatments. *J. Alloys Compd.* **2022**, *918*, 165748. doi:10.1016/j.jallcom.2022.165748
48. Pozdniakov, A.V.; Barkov, R.Yu. Effects of impurities on the phase composition and properties of a new alloy of the Al-Y-Er-Zr-Sc system. *Metallurgist* **2019**, *63*, 79-86. doi:10.1007/s11015-019-00796-w
49. Pozdnyakov, A.V.; Osipenkova, A.A.; Popov, D.A.; Makhov, S.V.; Napalkov, V.I. Effect of low additions of Y, Sm, Gd, Hf and Er on the structure and hardness of alloy Al-0.2%Zr-0.1%Sc. *Met. Sci. Heat Treat.* **2017**, *58*, 537–542, doi:10.1007/s11041-017-0050-z
50. Mochugovskiy, A.G.; Barkov, R.Yu.; Mikhaylovskaya, A.V.; Loginova, L.S.; Yakovtseva, O.A.; Pozdniakov, A.V. Structure and properties of Al-4.5Mg-0.15Zr compositions alloyed with Er, Y, and Yb. *Phys. Metals Metallogr.* **2022**, *123*, 466-473. doi:10.1134/S0031918X22050088

51. Barkov, R.Yu.; Mikhaylovskaya, A.V.; Yakovtseva, O.A.; Loginova, I.S.; Prosviryakov, A.S.; Pozdniakov, A.V. Effects of thermomechanical treatment on the microstructure, precipitation strengthening, internal friction, and thermal stability of Al-Er-Yb-Sc alloys with good electrical conductivity. *J. Alloys Compd.* **2021**, *855*, 157367. doi:10.1016/j.jallcom.2020.157367
52. Pozdniakov, A.V.; Aitmagambetov, A.R.; Makhov, S.V.; Napalkov, V.I. Effect of impurities of Fe and Si on the structure and strengthening upon annealing of the Al-0.2%Zr-0.1%Sc alloys with and without Y additive. *Phys. Metals Metallogr.* **2017**, *118*, 479-484. doi:10.1134/S0031918X17050118
53. Pozdniakov, A.V.; Barkov, R.Yu.; Prosviryakov, A.S.; Churyumov, A.Yu.; Golovin, I.S.; Zolotorevskiy, V.S. Effect of Zr on the microstructure, recrystallization behavior, mechanical properties and electrical conductivity of the novel Al-Er-Y alloy. *J. Alloys Compd.* **2018**, *765*, 1-6. doi:10.1016/j.jallcom.2018.06.163
54. Barkov, R.Yu.; Yakovtseva, O.A.; Mamzurina, O.I.; Loginova, I.S.; Medvedeva, S.V.; Prosviryakov, A.S.; Mikhaylovskaya, A.V., Pozdniakov, A.V. Effect of Yb on the structure and properties of an electroconductive Al-Y-Sc alloy. *Phys. Metals Metallogr.* **2020**, *121*, 604-609. doi:10.1134/S0031918X20060022
55. Tang, C.-I.; Zhou, D.-J. Precipitation hardening behavior of dilute binary Al-Yb alloy. *Transact. Nonferr. Met. Soc. China* **2014**, *24*, 2326-2330. doi:10.1016/S1003-6326(14)63352-5
56. Wu, H.; Zhang, Q.; Li, L.; Huang, M.; Zheng, Z.; Wen, S. Thermal stability of the precipitates in dilute Al-Er-Zr/Hf alloys at elevated temperatures. *Metals* **2022**, *12*, 1242. doi:10.3390/met12081242
57. Nokhrin, A.; Shadrina, I.; Chuvil'deev, V.; Kopylov, V. Study of structure and mechanical properties of fine-grained aluminum alloys Al-0.6wt.%Mg-Zr-Sc with ratio Zr:Sc = 1.5 obtained by cold drawing. *Materials* **2019**, *12*, 316. doi:10.3390/ma12020316
58. Nokhrin, A.V.; Shadrina, I.S.; Chuvil'deev, V.N.; Kopylov, V.I.; Berendeev, N.N.; Murashov, A.A.; Bobrov, A.A.; Tabachkova, N.Yu.; Smirnova, E.S.; Faddeev, M.A. Investigation of thermal stability of microstructure and mechanical properties of bimetallic fine–grained wires from Al–0.25%Zr–(Sc,Hf) alloys. *Materials* **2022**, *15*, 185. doi:10.3390/ma15010185
59. Chuvil'deev; V.N.; Shadrina, Ya.S.; Nokhrin, A.V.; Kopylov, V.I.; Bobrov, A.A.; Gryaznov, M.Yu.; Shotin, S.V.; Tabachkova, N.Yu.; Chegurov, M.K.; Melekhin, N.V. An investigation of thermal stability of structure and mechanical properties of Al-0.5Mg-Sc ultrafine-grained aluminum alloys. *J. Alloys Compd.* **2020**, *831*, 154805. doi:10.1016/j.jallcom.2020.154805
60. Chuvil'deev, V.N.; Nokhrin, A.V.; Makarov, I.M.; Lopatin, Yu.G.; Sakharov, N.V.; Melekhin, N.V.; Piskunov, A.V.; Smirnova, E.S.; Kopylov, V.I. Solid solution decomposition mechanisms in cast and microcrystalline Al-Sc alloys: I. Experimental studies. *Russian Metallurgy (Metally)* **2012**, *5*, 415-427. doi:10.1134/S0036029512050084
61. Zakharov, V.V. Prospects of creation of aluminum alloys sparingly alloyed with scandium. *Met. Sci. Heat Treat.* **2018**, *60*, 172-176. doi:0.1007/s11041-018-0256-8
62. Zakharov, V.V. Stability of the solid solution of scandium in aluminum. *Met. Sci. Heat Treat.* **1997**, *39*, 61-66. doi:10.1007/bf02467664
63. Zakharov, V.V. Cobmined alloying of aluminum alloys with scandium and zirconium. *Met. Sci. Heat Treat.* **2014**, *56*, 281–286. doi:10.1007/s11041-014-9746-5
64. Røyset, J.; Ryum, N. Scandium in aluminum alloys. *Int. Mater. Rev.* **2005**, *50*, 19-44. doi:10.1179/174328005X14311
65. Filatov, Yu.A.; Elagin, V.I.; Zakharov, V.V. New Al-Mg-Sc alloys. *Mater. Sci. Eng. A* **2000**, *280*, 97-101. doi:10.1016/S0921-5093(99)00673-5
66. Davydov, V.G.; Rostova, T.D.; Zakharov, V.V.; Filatov, Yu.A.; Yelagin, V.I. Scientific principles of making an alloying of scandium to aluminium alloys. *Mater. Sci. Eng. A* **2000**, *280*, 30-36. doi:10.1016/S0921-5093(99)00652-8
67. Eskin, D.G. Sc applications in aluminum alloys: Overview of Russian research in the 20th century. *Minerals, Metals and Materials Series* **2018**, *F4*, 1565-1572. doi:10.1007/978-3-319-72284-9_204
68. Latynina, T.A.; Mavlyutov, A.M.; Valiev, R.Z.; Murashkin, M.Y.; Orlova, T.S. The effect of hardening by annealing in ultrafine-grained Al-0.4Zr alloy: Influence of Zr microadditives. *Philos. Mag.* 2019, *99*, 2424–2443, doi:10.1080/14786435.2019.1631501.
69. Belov, N.; Korotkova, N.; Akopyan, T.; Murashkin, M.; Timofeev, V. Structure and properties of Al-0.6wt.%Zr wire alloy manufactured by direct drawing of electromagnetically cast wire rod. *Metals* **2020**, *10*, 769. doi:10.3390/met10060769
70. Mohammadi, A.; Enikeev, N.A.; Murashkin, M.Yu.; Arita, M.; Edalati, K. Developing age-hardenable Al-Zr alloy by ultra-severe plastic deformation: Significance of supersaturation, segregation and precipitation on hardening and electrical conductivity. *Acta Mater.* **2021**, *203*, 116503. doi:10.1016/j.actamat.2020.116503
71. Orlova, T.S.; Latynina, T.A.; Mavlyutov, A.M.; Murashkin, M.Y.; Valev, R.Z. Effect of annealing on microstructure, strength and electrical conductivity of the pre-aged and HPT-processed Al-0.4Zr alloy. *J. Alloys Compd.* **2019**, *784*, 41-48. doi:10.1016/j.jallcom.2018.12.324
72. Belov, N.A.; Alabin, A.N.; Yakovlev, A.A. Influence of the annealing temperature on the phase composition of Al-0.55 wt%Zr cast alloy. *Russ. J. Non-Ferr. Met.* **2013**, *54*, 224–228. doi:10.3103/S1067821213030048
73. Belov, N.A.; Korotkova, N.O.; Akopyan, T.K.; Timofeev, V.N. Structure and properties of Al-0.6%Zr-0.4%Fe-0.4%Si (wt.%) wire alloy manufactured by electromagnetic casting. *JOM* **2020**, *72*, 1561–1570. doi:10.1007/s11837-019-03875-0
74. Orlova, T.S.; Mavlyutov, A.M.; Latynina, T.A.; Ubyivovk, E.V.; Murashkin, M.M.; Schneider, R.; Gerthsen, D.; Valiev, R.Z. Influence of severe plastic deformation on microstructure, strength and electrical conductivity of aged Al-0.4Zr (wt.%) alloy. *Rev. Adv. Mater. Sci.* **2018**, *55*, 92-101. doi:10.1515/rams-2018-0032

75. Voroshilov, D.S.; Motkov, M.M.; Sidelnikov, S.B.; Sokolov, R.E.; Durnopyanov, A.V.; Konstantionov, I.L.; Bespalov, V.M.; Bermeshev, T.V.; Gudkov, I.S.; Voroshilova, M.V.; Mansurov, Y.N.; Berngard, V.A. Obtaining Al-Zr-Hf wire using electromagnetic casting, combined rolling-extrusion, and drawing. *Int. J. Ligh. Mater. Manufact.* **2022**, *5*, 352-368. doi:10.1016/j.ijlmm.2022.04.002
76. Zhang, J.; Wang, H.; Yi, D.; Wang, B.; Wang, H. Comparative study of Sc and Er addition on microstructure, mechanical properties, and electrical conductivity of Al-0.2Zr-based alloy cables. *Mater. Charact.* **2018**, *145*, 126-134. doi:10.1016/j.matchar.2018.08.037
77. Michi, R.A.; De Luca, A.; Seidman, D.N.; Dunand, D.C. Effects of Si and Fe micro-additions on the aging response of a dilute Al-0.08Zr-0.08Hf-0.045Er at.% alloy. *Mater. Charact.* **2019**, *147*, 72-83. doi:10.1016/j.matchar.2018.10.016
78. Wen, S.P.; Gao, K.Y.; Li, Y.; Huang, H.; Nie, Z.R. Synergetic effect of Er and Zr on the precipitation hardening of Al-Er-Zr alloy. *Scr. Mater.* **2011**, *65*, 592–595, doi:10.1016/j.scriptamat.2011.06.033
79. Mochegovskiy, A.G.; Mikhaylovskaya, A.V.; Tabachkova, N.Yu.; Portnoy, V.K. The mechanism of $L1_2$ precipitation, microstructure and tensile properties of Al-Mg-Er-Zr alloy. *Mater. Sci. Eng. A* **2019**, *744*, 195-205. doi:10.1016/j.msea.2018.11.135
80. Li, H.; Gao, Z.; Yin, H.; Jiang, H.; Su, X.; Bin, J. Effects of Er and Zr additions on precipitation and recrystallization of pure aluminum. *Scr. Mater.* **2013**, *68*, 59-62. doi:10.1016/j.scriptamat.2012.09.026
81. Wen, S.P.; Gao, K.Y.; Huang, H.; Wang, W.; Nie, Z.R. Precipitation evolution in Al-Er-Zr alloys during aging at elevated temperature. *J. Alloys Compd.* **2013**, *574*, 92-97. 10.1016/j.jallcom.2013.03.237
82. Kotov, A.D.; Mochugovskiy, A.G.; Mosleh, A.O.; Kishchik, A.A.; Rofman, O.V.; Mikhaylovskaya, A.V. Microstructure, superplasticity, and mechanical properties of Al-Mg-Er-Zr alloys. *Mater. Charact.* **2022**, *186*, 111825. doi:10.1016/j.matchar.2022.111825
83. Wen, S.P.; Wang, W.; Zhao, W.H.; Wu, X.L.; Gao, K.Y.; Huang, H.; Nie, Z.R. Precipitation hardening and recrystallization behavior of Al-Mg-Er-Zr alloys. *J. Alloys Compd.* **2016**, *687*, 143-151. doi:10.1016/j.jallcom.2016.06.045
84. Gao, H.; Feng, W.; Gu, J.; Wang, J.; Sun, B. Aging and recrystallization behavior of precipitation strengthened Al-0.25Zr-0.03Y alloy. *J. Alloys Compd.* **2017**, *696*, 1039-1045. 10.1016/j.jallcom.2016.12.064
85. Gao, H.; Feng, W.; Wang, Y.; Gu, J.; Zhang, Y.; Wang, J.; Sun, B. Structural and compositional evolution of $Al_3(Zr,Y)$ precipitates in Al-Zr-Y alloy. *Mater. Charact.* **2016**, *121*, 195-198. doi:10.1016/j.matchar.2016.10.012
86. Zhang, Y.; Gu, J.; Tian, Y.; Gao, H.; Wang, J.; Sun, B. Microstructural evolution and mechanical properties of Al-Zr and Al-Zr-Y alloys. *Mater. Sci. Eng. A* **2014**, *616*, 132-140. doi:10.1016/j.msea.2014.08.017
87. Zhang, Y.; Gao, H.; Kuai, Y.; Han, Y.; Wang, J.; Sun, B.; Gu, S.; You, W. Effects of Y additions on the precipitation and recrystallization of Al-Zr alloys. *Mater Charat.* **2013**, *86*, 1-8. doi:10.1016/j.matchar.2013.09.004
88. Zhang, Y.; Zhou, W.; Gao, H.; Han, Y.; Wang, K.; Wang, J.; Sun, B.; Gu, S.; You, W. Precipitation evolution of Al-Zr-Yb alloys during isochronal aging. *Scr. Mater.* **2013**, *69*, 477-480. doi:10.1016/j.scriptamat.2013.06.003
89. Peng, G.; Chen, K.; Fang, H.; Chen, S. A study of nanoscale $Al_3(Zr,Yb)$ dispersoids structure and thermal stability in Al-Zr-Yb alloys. *Mater. Sci. Eng. A* **2012**, *535*, 311-315. doi:10.1016/j.msea.2011.12.094
90. Wen, S.P.; Gao, K.Y.; Huang, H.; Wang, W.; Nie, Z.R. Role of Yb and Si on the precipitation hardening and recrystallization of dilute Al-Zr alloy. *J. Alloys Compd.* **2014**, *599*, 65–70, doi:10.1016/j.jallcom.2014.02.065
91. Nes, E.; Ryum, N. On the formation of fan-shaped precipitates during the decomposition of a highly supersaturated Al-Zr solid solution. *Scripta Mater.* **1971**, *5*, 987-989. doi:10.1016/0036-9748(71)90142-6
92. Nes, E.; Billdal, H. The mechanism of discontinuous precipitation of the metastable Al_3Zr phase from an Al-Zr solid solution. *Acta Metall.* **1977**, *25*, 1039-1046. doi:10.1016/0001-6160(77)90133-X
93. Mikhaylovskaya, A.V.; Mochugovskiy, A.G.; Levchenko, V.S.; Tabachkova, N.Yu.; Mufalo, W.; Portnoy, V.K. Precipitation behavior of $L1_2$ Al_3Zr phase in Al-Mg-Zr alloy. *Mater. Charat.* **2018**, *139*, 30-37. doi:10.1016/j.matchar.2018.02.030
94. Mochugovskiy, A.G.; Mikhaylovskaya, A.V. Comparison of precipitation kinetics and mechanical properties in Zr and Sc-bearing aluminum-based alloys. *Mater. Lett.* **2020**, *275*, 128096. doi:10.1016/j.matlet.2020.128096
95. Mochugovskiy, A.G.; Mikhaylovskaya, A.V.; Zadorognyy, M.Yu.; Golovin, I.S. Effect of heat treatment on the grain size control, superplasticity, internal friction, and mechanical properties of zirconium-bearing aluminum-based alloy. *J. Alloys Compd.* **2021**, *856*, 157455. doi:10.1016/j.jallcom.2020.157455
96. Schmid, F.; Gehringer, D.; Kremmer, T.; Cattini, L.; Uggowitzer, P.J.; Holec, D.; Pogatscher, S. Stabilization of Al_3Zr allotropes in dilute aluminum alloys via the addition of ternary elements. *Materialia* **2022**, *21*, 101321. doi:10.1016/j.mtla.2022.101321
97. Chuvil'deev, V.N.; Nokhrin, A.V.; Smirnova, E.S.; Kopylov, V.I. Solid solution decomposition mechanisms in cast and microcrystalline Al-Sc alloys: III. Analysis of experimental data. *Russian Metallurgy (Metally)* **2012**, *11*, 985-993. doi:10.1134/S0036029512110031
98. Shamtko, O.A.; Usov, Y.V. *Structure and properties of metals and alloys. Electrical and magnetic properties of metals*. Naukova Dumka: Kiev, USSR, 1987, 325 p. (in Russian)
99. Chuvil'deev, V.N.; Smirnova, E.S.; Kopylov, V.I. Solid solution decomposition mechanisms in cast and microcrystalline Al-Sc alloys: II. Model for the decomposition of a solid solution during the formation of coherent second-phase particles. *Russian Metallurgy (Metally)* **2012**, *7*, 612-624.doi:10.1134/S0036029512070063
100. Christian, J.W. *The theory of transformations in metals and alloys. Part I. Equilibrium and General Kinetic Theory*. Pergamon Press: Oxford, UK, 2002, 1200 p.

 doi:10.20944/preprints202212.0407.v1

101. Martin, J.W. *Micromechanisms in particle-hardened alloys*. Cambridge Univ. Press: Cambridge, UK, 1980, 167 p.
102. Chuvil'deev, V.N.; Nokhrin, A.V.; Smirnova, E.S.; Kopylov, V.I. Solid solution decomposition mechanisms in as-cast and microcrystalline Al-Sc alloys: IV. Effect of the decomposition of a solid solution on the mechanical properties of the alloys. *Russian Metallurgy (Metally)* **2013**, *9*, 676-690. doi:10.1134/S0036029513090061